Evaporation tagging and atmospheric water budget analysis with WRF: A regional precipitation recycling study for West Africa

Joel Arnault, Hans Richard Knoche, Jianhui Wei, Harald Kunstmann

Angaben zur Veröffentlichung / Publication details:

Arnault, Joel, Hans Richard Knoche, Jianhui Wei, and Harald Kunstmann. 2016. "Evaporation tagging and atmospheric water budget analysis with WRF: A regional precipitation recycling study for West Africa." *Water Resources Research* 52 (3): 1544–67. https://doi.org/10.1002/2015WR017704.

AGU PUBLICATIONS

Water Resources Research

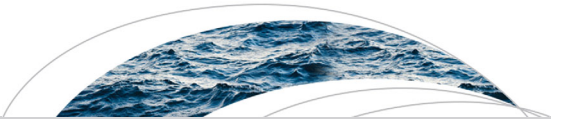

RESEARCH ARTICLE

10.1002/2015WR017704

Key Points:
- Evaporation tagging and budgets of atmospheric water species are implemented in WRF
- Return flow strengthens scale-dependency of regional precipitation recycling in West Africa
- Local evaporation in West Africa is not the dominant factor controlling local precipitation

Supporting Information:
- Movie S1

Correspondence to:
J. Arnault,
joel.arnault@kit.edu

Citation:
Arnault, J., R. Knoche, J. Wei, and H. Kunstmann (2016), Evaporation tagging and atmospheric water budget analysis with WRF: A regional precipitation recycling study for West Africa, *Water Resour. Res.*, *52*, 1544–1567, doi:10.1002/2015WR017704.

Received 16 JUN 2015
Accepted 28 JAN 2016
Accepted article online 2 FEB 2016
Published online 4 MAR 2016

Evaporation tagging and atmospheric water budget analysis with WRF: A regional precipitation recycling study for West Africa

Joel Arnault[1,2], Richard Knoche[1], Jianhui Wei[1,2], and Harald Kunstmann[1,2]

[1]Karlsruhe Institute of Technology, Institute of Meteorology and Climate Research, Garmisch-Partenkirchen, Germany, [2]Institute of Geography, Chair for Regional Climate and Hydrology, University of Augsburg, Augsburg, Germany

ABSTRACT Regional precipitation recycling is the measure of the contribution of local evaporation E to local precipitation. This study provides a set of two methods developed in the Weather Research and Forecasting WRF model system for investigating regional precipitation recycling mechanisms: (1) tracking of tagged atmospheric water species originating from evaporation in a source region, ie E-tagging, and (2) three-dimensional budgets of total and tagged atmospheric water species. These methods are used to quantify the effect of return flow and nonwell vertical mixing neglected in the computation of the bulk precipitation recycling ratio. The developed algorithms are applied to a WRF simulation of the West African Monsoon 2003. The simulated region is characterized by vertical wind shear condition, i.e., southwesterlies in the low levels and easterlies in the mid-levels, which favors return flow and nonwell vertical mixing. Regional precipitation recycling is investigated in 100 × 100 and 1000 × 1000 km^2 areas. A prerequisite condition for evaporated water to contribute to the precipitation process in both areas is that it is lifted to the mid-levels where hydrometeors are produced. In the 100 × 100 (1000 × 1000) km^2 area the bulk precipitation recycling ratio is 0.9 (7.3) %. Our budget analysis reveals that return flow and nonwell vertically mixed outflow increase this value by about +0.2 (2.9) and +0.2 (1.6) %, respectively, thus strengthening the well-known scale-dependency of regional precipitation recycling.

1. Introduction

The concept of regional precipitation recycling, i.e., measure of the contribution of local evaporation *E* to local precipitation [*Van der Ent and Savenije*, 2011], aims at studying the atmospheric branch of the water cycle [*Eltahir and Bras*, 1996]. It has been extensively used for quantifying the dependency of local climate on the land surface [e.g., *Brubaker et al*., 1993; *Eltahir and Bras*, 1996; *Dirmeyer and Brubaker*, 1999; *Trenberth*, 1999; *Bosilovich and Schubert*, 2001; *Burde and Zangvil*, 2001; *Van der Ent et al*., 2010; *Goessling and Reick*, 2011; *Gimeno et al*., 2012]. The knowledge of the relationship between local precipitation and land surface characteristics would indeed be highly valuable for land use management in the context of climate change [*Savenije*, 1995]. This is particularly relevant for regions threatened by droughts and characterized by a primarily rainfed agriculture, such as West Africa [*Nicholson*, 2000].

As highlighted by *Trenberth* [1999] regional precipitation recycling depends greatly on the scale of the domain under consideration and on the atmospheric circulation, so that at the 1000 × 1000 km^2 scale generally less than 20% of the annual local precipitation typically comes from local *E*. Moreover, high regional precipitation recycling is generally found where moisture transport is weak and precipitation is convective [*Bosilovich and Schubert*, 2001; *Bosilovich et al*., 2003; *Bosilovich and Chern*, 2006; *Dominguez et al*., 2008; *Dominguez and Kumar*, 2008; *Bisselink and Dolman*, 2008; *Pathak et al*., 2014; *Rios-Entenza et al*., 2014].

Druyan and Koster [1989] investigated the particular case of regional precipitation recycling in West Africa. Using two different climatological data sets they initialized two global atmospheric simulations for the month of July, one producing dry and the other wet conditions in this region. Tracking water vapor evaporating from predefined areas online in the numerical simulation, i.e., a method known as *E*-tagging [*Joussaume et al*., 1986; *Koster et al*., 1986], *Druyan and Koster* [1989] found regional precipitation recycling ratios of 30 and 15% in a 2000 × 2000 km^2 West African area for the wet and dry cases, respectively. According to *Druyan and Koster* [1989], however, differences in simulated West African precipitation between the two

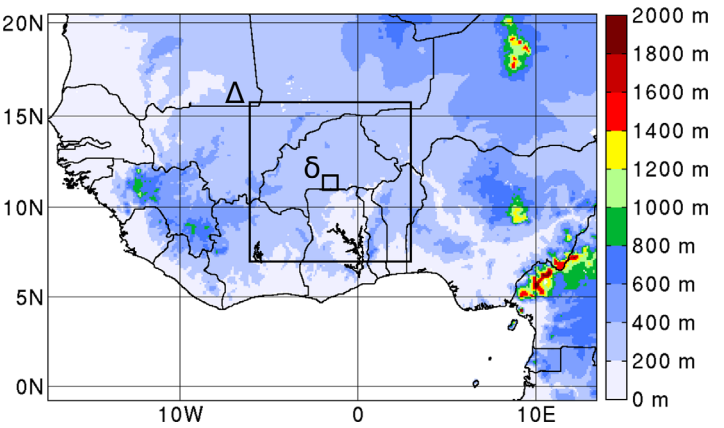

Figure 1. Terrain elevation (m a.s.l.) of the 10 km-resolution WRF domain. The height scale is given by the coloured bar to the right. The curved black lines delineate the West African coast and the political boundaries. The black squares show the location of domain δ (100 $\times$ 100 km^2) and domain Δ (1000 $\times$ 1000 km^2) discussed in the text.

simulations were mainly caused by the atmospheric circulation favoring convergence of oceanic moisture over West Africa in the wet case, but not in the dry one.

In the West African region situated between the wet Guinean Coast and the dry Saharan desert, rainfall strongly influences the spatial distribution of soil moisture and surface fluxes [*Taylor et al.*, 2007, 2011a], which eventually affects subsequent precipitation events [e.g., *Gantner and Kalthoff*, 2010; *Taylor et al.*, 2011b]. *Kunstmann and Jung* [2007] tested the impact of reduced and increased soil moisture initial condition in a regional atmospheric simulation over West Africa for a 1 month period in July–August 1998, with the Mesoscale Model MM5 [*Grell et al.*, 1994]. The dependency of the so-called bulk precipitation recycling ratio β_{bulk} from *Schär et al.* [1999] to soil moisture initial condition was investigated (for the definition of β_{bulk} it is referred to section 3). β_{bulk} appeared to be an increasing function of this soil moisture initial condition, until a threshold after which it remained almost constant. In the latter case, β_{bulk} was around 6.7 and 12.5% for 1000 $\times$ 600 and 1600 $\times$ 1600 km^2 areas, respectively.

β_{bulk} is generally computed offline at a relatively low temporal resolution and relies on the hypothesis that the atmospheric flow is two-dimensional. More particularly, this hypothesis implies that (1) moisture species originating from inside and transported outside of the source area do not return back, i.e., no return flow, (2) moisture species originating from *E* inside and outside the source area are well mixed [*Schär et al.*, 1999]. As shown by *Goessling and Reick* [2013] the hypothesis of well vertical mixing is however seldom met, especially when vertical wind shear is strong, leading to substantial error in evaluating regional precipitation recycling with such a two-dimensional method.

In comparison to less computationally expensive offline methods, online *E*-tagging was recently considered as one of the most suitable method to investigate regional precipitation recycling in regions characterized by sharp vertical wind shear, such as West Africa [*Van der Ent et al.*, 2013]. An *E*-tagging method was recently implemented in MM5 by *Knoche and Kunstmann* [2013] and further developed by *Wei et al.* [2015]. Applying *E*-tagging in a simulation over West Africa for July–August 1998, *Knoche and Kunstmann* [2013] tracked soil moisture evaporating from a 160 $\times$ 250 km^2 area around Lake Volta until precipitation or transport outside of the model domain. They found that evaporating water from Lake Volta was generally transported northeastward in the low levels by the oceanic monsoon flow, although convective processes allowed some of this tagged water vapor to be lifted and then transported westward by the mid-level African Easterly Jet (AEJ) before eventually precipitating in the source area. This mechanism is referred as the atmospheric water pathway from *Knoche and Kunstmann* [2013] in the following analysis. It was finally found that about 1.7% of the evaporated water in the source area locally recycled as precipitation.

The present study aims at further investigating atmospheric processes involved in regional precipitation recycling, i.e., the atmospheric branch of the water cycle, in West Africa. The *E*-tagging method of *Knoche and Kunstmann* [2013] is for the first time now implemented in the Weather Research and Forecasting (WRF) model [*Skamarock and Klemp*, 2008]. An online budget analysis of total and tagged atmospheric water species adapted from *Arnault* [2013] is additionally implemented. These three-dimensional budgets are subsequently used to derive an online version of the vertically integrated, i.e., bulk, atmospheric moisture budget from *Schär et al.* [1999], and quantify the contribution of three-dimensional atmospheric processes neglected in the computation of β_{bulk}, i.e., return flow and nonwell vertical mixing.

The West African Monsoon of the year 2003 is simulated for a domain covering West Africa and the surrounding Atlantic Ocean (see the simulated WRF domain in Figure 1). Scale dependency of regional precipitation recycling mechanisms is addressed by applying *E*-tagging and budget analyses to two source regions, a 100 $\times$ 100 km^2 area around (11.5°N 1.5°S) in the West African Sudanian region, referred as domain δ, and a 1000 $\times$ 1000 km^2 area centered on domain δ, referred as domain Δ (see Figure 1).

Section 2 presents our WRF setup and a validation of simulated precipitation and evaporation. Our quantitative methods to analyze regional precipitation recycling mechanisms are detailed in section 3. Results for domains δ and Δ are provided in sections 4 and 5, respectively. A summary and conclusion is finally given in section 6.

2. Modeled Case Study

2.1. Numerical Set-Up

The WRF model used in this study is based on the standard version 3.5.1 (available at: http://www2.mmm.ucar.edu/wrf/users/downloads.html) upgraded with the online computation of *E*-tagging and budgets of total and tagged atmospheric water species detailed in section 3. Our WRF simulation consists of one Mercator projected domain at 10 km resolution (Figure 1) covering a sufficiently large area to the South (1.2°S–20.8°N) and to the East (17.8°W–13.8°E), in order to resolve the oceanic monsoon flow and African Easterly Wave disturbances, two important factors controlling West African monsoonal precipitation [*Browne and Sylla*, 2012]. The vertical grid consists of 35 vertical levels up to 20 hPa (approximately 25 km), with a vertical spacing stretched from 70 to 1000 m at the lowest and highest level, respectively. Radiative processes are represented with the long and short-wave radiation schemes of *Mlawer et al.* [1997] and *Dudhia* [1989], respectively. Microphysics is parameterized with the five-class liquid and ice hydrometeors scheme of *Hong et al*. [2004]. The cumulus scheme has been switched off since the 10 km resolution appears to be high enough to simulate West African precipitation characteristics comparable to that derived from satellite observation [e.g., *Marsham et al*., 2013] (see section 3).

Horizontal subgrid transport of heat, moisture and momentum is determined with a horizontal first order Smagorinsky closure, and the vertical subgrid transport of the same quantities is parameterized in the whole atmospheric column with the scheme of *Hong et al*. [2006]. Surface exchange coefficients are computed according to *Chen and Zhang* [2009] in order to take into account the effect of canopy height on land-atmosphere exchanges. Surface heat and moisture fluxes are calculated with the Noah Land Surface Model (LSM) predicting soil temperature and soil moisture in a 2 m-depth four-layer column and taking into account vegetation effects [*Chen and Dudhia*, 2001]. Albedo, vegetation fraction and leaf area index (LAI) are taken from satellite-derived climatology [*Csiszar and Gutman*, 1999; *Gutman and Ignatov*, 1998; *Kumar et al*., 2014], whereas other land surface parameters are assigned for each land category from the moderate resolution imaging spectroradiometer (MODIS) land cover map [*Friedl et al*., 2002].

The simulated WRF domain is forced with the 0.75°-resolution ERA-interim reanalyzes [*Dee et al*., 2011] at the initial time and every 6 h at the lateral boundaries. Model equations are integrated at a time step of 50 s. Model outputs containing usual atmospheric and surface variables, as well as the tagged water species and the integrated terms of the budget equations presented in section 3, are saved at a 3 h interval. This WRF setup is run two times for the wet season March–October 2003 with a 2 -month spin-up period, a first time with domain δ as source region for *E*-tagging, and a second time with domain Δ (see Figure 1). These two simulations are identical, except for the tagged water species.

2.2. Model Versus Observation

Simulated precipitation *P* and evaporation *E* are compared here with observational data sets from the Tropical Rainfall Measuring Mission (TRMM) [*Huffman et al*., 2007] and from the Model Tree Ensemble (MTE) [*Jung et al*., 2009, 2010], respectively.

TRMM data set is a merged product from remote-sensing and in-situ measurements, available 3 hourly at 0.25° resolution for the simulated period from March to October 2003. It is a commonly used product for evaluating West African precipitation [e.g., *Nicholson et al*., 2003; *Browne and Sylla*, 2012; *Thiemig et al*., 2012; *Marsham et al*., 2013; *Klein et al*., 2015]. MTE data set is also a merged product, available monthly at 0.5°

resolution for the considered period. Timeseries of monthly P and E spatially averaged in domains δ and Δ, as well as histogram of daily P, are shown in Figure 2.

In domain δ, monthly P from WRF is higher (lower) than that from TRMM in May, July, and August (in June, September, and October) (Figure 2a), leading to a monthly root mean square error (RMSE) of 1.8 mm d^{-1} and a difference between modeled and observed total P of +8.3%. In comparison, monthly E from WRF is much closer to that from MTE (Figure 2b), with a monthly RMSE of 0.4 mm d^{-1} and a difference between modeled and observed total E of −2.8%. WRF- and observation-derived ratios between total E and total P are 48 and 54%, respectively (Table 1). At the daily scale, the correlation coefficient between WRF and TRMM P is 0.27. This is related to the fact that precipitation is mainly convective in West Africa, and that the location of convective cells may not always be well captured by the model at the scale of domain δ (i.e., 100 × 100 km^2). WRF and TRMM histograms of daily P are on the other hand relatively close (Figure 3b), with a clear overestimation of simulated high precipitation events, i.e., above 35 mm d^{-1}.

In domain Δ, WRF-derived monthly P is closer to that from TRMM (Figure 2d), with a monthly RMSE of 0.4 mm d^{-1} and a difference in the total P of +4.5%. Monthly E from WRF and MTE are also relatively close (Figure 2e), with a monthly RMSE of 0.2 mm d^{-1} and a difference in the total E of + 1.1% (Table 1). As compared to domain δ, E in domain Δ is lower, in relation with the fact that domain Δ includes a larger proportion of dryer areas to the North, closer to the Saharan region (Figure 2d and Table 1). WRF- and observation-derived ratios between total E and total P in domain Δ are on the other hand similar to that in domain δ (Table 1). Modeled and observed daily P in domain Δ are also closer, with a correlation coefficient of 0.62 and relatively close histograms (Figure 3f).

It is concluded here that modeled P and E are reproduced reasonably and that our WRF simulation allows to study P- and E-related processes like regional precipitation recycling mechanisms.

3. Quantitative Methods

3.1. Budget of Atmospheric Water Species

It is recalled that the WRF model [*Skamarock and Klemp*, 2008] resolves the nonhydrostatic compressible equations of motion in their flux form using a terrain-following hydrostatic pressure (mass) vertical coordinate $\eta=(p_h-p_{ht})/(p_{hs}-p_{ht})=(p_h-p_{ht})/\mu$, where p_h is the hydrostatic pressure, p_{ht} and p_{hs} are the hydrostatic pressures at the top and surface of the model, respectively, and $\mu=p_{hs}-p_{ht}$ represents the mass of the dry air per unit area within the modeled atmospheric column. In our WRF setup microphysical processes are explicitly resolved with the five-class liquid and ice hydrometeors microphysics scheme of *Hong et al.* [2004]. The five prognostic variables of this scheme are the mixing ratio of water vapor q_v, cloud droplet q_c, rain droplet q_r, ice particles q_i and snow particles q_s. Considering q_H as the sum of the mixing ratio of liquid and ice hydrometeors, the flux-form microphysical equations resolved in our WRF setup can be written as

$$\underbrace{(\mu\cdot q_v)_t}_{a1}=\underbrace{-\left[(U\cdot q_v)_x+(V\cdot q_v)_y+(\Omega\cdot q_v)_\eta\right]}_{a2}+\underbrace{\mu\cdot\left(F_{qv}^H+F_{qv}^V\right)}_{a3}+\underbrace{\mu\cdot C}_{a4} \quad (1)$$

$$\underbrace{(\mu\cdot q_H)_t}_{b1}=\underbrace{-\left[(U\cdot q_H)_x+(V\cdot q_H)_y+(\Omega\cdot q_H)_\eta\right]}_{b2}+\underbrace{\mu\cdot\left(F_{qH}^H+F_{qH}^V\right)}_{b3}\underbrace{-\mu\cdot C}_{b4}+\underbrace{\mu\cdot P_H}_{b5} \quad (2)$$

where u, v, w are the three-dimensional components of the wind; $U=\mu\cdot u$, $V=\mu\cdot v$ and $\Omega=\mu\cdot(g\cdot w-\Phi_x\cdot u-\Phi_y\cdot v)$ are the contravariant components of the momentum in the coordinate system of the model (x, y, η); subscripts x, y, η and t stand for the derivate operators in the three directions of this coordinate system and the time derivate operator; Φ is the geopotential and g the acceleration of gravity; F_{qv}^H, F_{qH}^H, (F_{qv}^V, F_{qH}^V) are the subgrid horizontal (vertical) transport terms; C stands for the phase changes between q_v and q_H; and P_H is the fallout of hydrometeors. In equation (1), the tendency of $\mu\cdot q_v$ (a1) is equal to the sum of grid-resolved horizontal and vertical transport of $\mu\cdot q_v$ (a2), subgrid horizontal and vertical transport of $\mu\cdot q_v$ (a3), and phase change (a4). Evaporation E is considered as the subgrid vertical fluxes of q_v at the lower boundary (see subgrid vertical transport scheme of *Hong et al.* [2006]), so that it is contained in the term F_{qv}^V in equation (1). In equation (2), the tendency of $\mu\cdot q_H$ (b1) is equal to the sum of grid-resolved horizontal and vertical transport

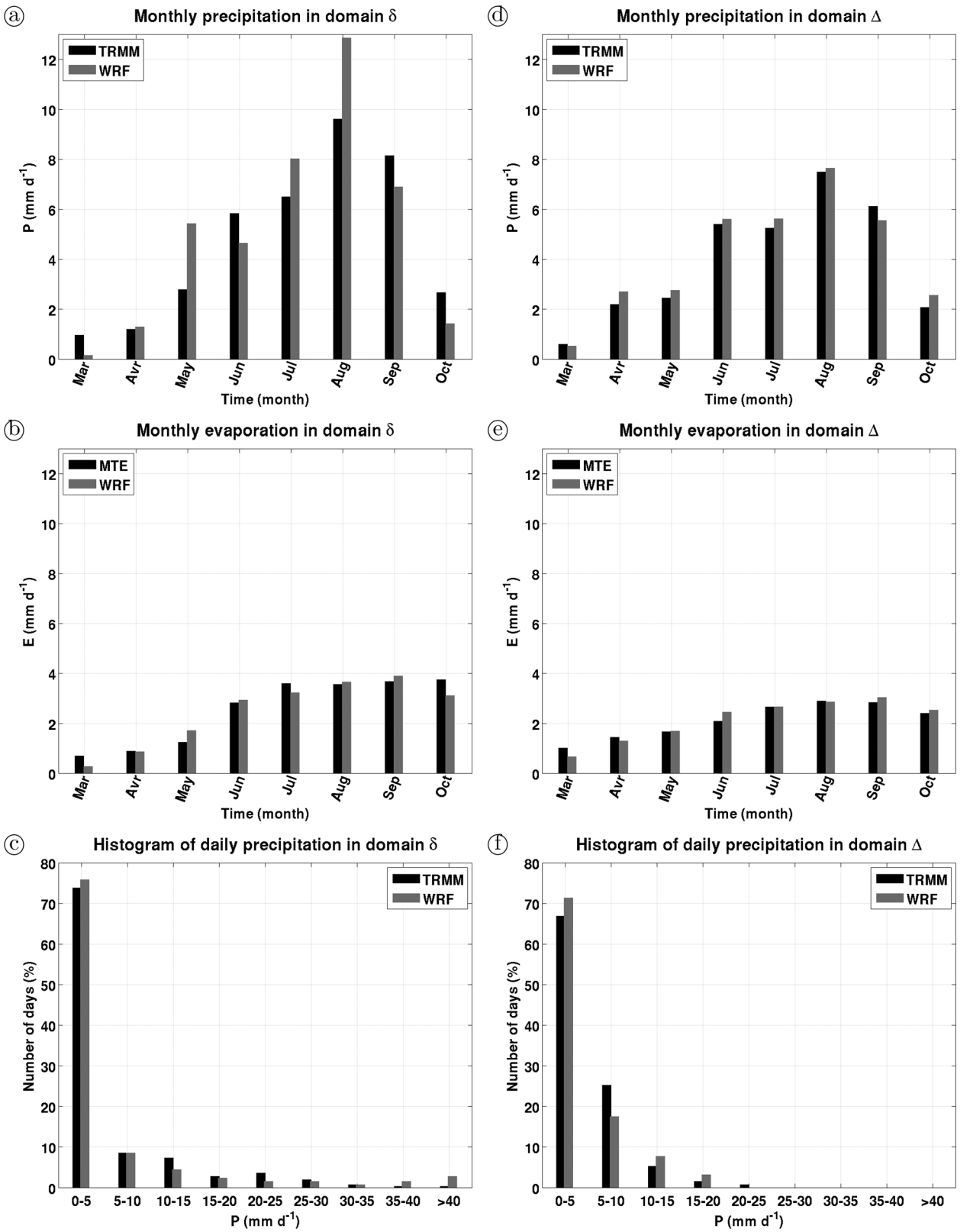

Figure 2. (a) Time-series of monthly precipitation P (mm d^{-1}) averaged in domain δ (see Figure 1), derived from TRMM (black bars) and from WRF (grey bars). The x axis gives the time from March to October 2003, and the y axis the precipitation amount. (b) As in Figure 2a, except for monthly evaporation E (mm d^{-1}) derived from MTE (black bars) and from WRF (grey bars). (c) Histograms of daily P averaged in domain δ derived from TRMM (black bars) and from WRF (grey bars). The x axis gives P bins in mm d^{-1}, and the y axis the number of days in percentages. (d-f) As in Figures 2a–2c, except for domain Δ.

Table 1. Total Precipitation and Evaporation Spatially Averaged in Domains δ and Δ[a]

	Domain δ	Domain Δ
P	**1157 mm**, *1253 mm (+8.3%)*	**968 mm**, *1011 mm (+4.5%)*
E	**624 mm**, *606 mm (−2.8%)*	**524 mm**, *530 mm (+1.1%)*
E/P	**54%**, *48%*	**54%**, *52%*

[a](Second row) Total precipitation P spatially averaged in domains δ and Δ shown in Figure 1 for the period March–October 2003, from the TRMM data set (in bold) and from the WRF simulation (in italic). Difference (%) between observed and modeled total P is given in parenthesis. (Third row) As in the second line, except for evaporation E from the MTE data set (in bold) and from the WRF simulation (in italic). (Fourth row) as in the second line, except for the ratio between total E and total P (%) from the observational data sets (in bold) and from the WRF simulation (in italic).

of $\mu{\cdot}q_H$ (b2), subgrid horizontal and vertical transport of $\mu{\cdot}q_H$ (b3), phase change (b4), and hydrometeors fallout (b5).

Budgets of q_v and q_H can be implemented online in WRF by integrating equations (1) and (2) at the model time step, using the same method developed by *Arnault* [2013] for implementing the budget of momentum in WRF. However, q_v and q_H, as mixing ratios, do not give the quantity of atmospheric water species. Since this work also aims at computing online the bulk atmospheric moisture budget from *Schär et al*. [1999] (see section 3.2), the following equations are more particularly considered for the budget implementation in WRF

$$\underbrace{(dz\cdot\rho_v)_t}_{c1}=\underbrace{dz\cdot\rho_d\cdot\mu^{-1}\cdot\left[-(U\cdot q_v)_x-(V\cdot q_v)_y+\mu\cdot F_{qv}^H\right]}_{c2}+\underbrace{dz\cdot\rho_d\cdot\mu^{-1}\cdot\left[-(\Omega\cdot q_v)_\eta+\mu F_{qv}^V\right]}_{c3}+\underbrace{dz\cdot\rho_d\cdot C}_{c4}+residual \tag{3}$$

$$\underbrace{(dz\cdot\rho_H)_t}_{d1}=\underbrace{dz\cdot\rho_d\cdot\mu^{-1}\cdot\left[-(U\cdot q_H)_x-(V\cdot q_H)_y+\mu\cdot F_{qH}^H\right]}_{d2}+\underbrace{dz\cdot\rho_d\cdot\mu^{-1}\cdot\left[-(\Omega\cdot q_H)_\eta+\mu\cdot F_{qH}^V\right]}_{d3}\underbrace{-dz\cdot\rho_d\cdot C}_{d4}+\underbrace{dz\cdot\rho_d\cdot P_H}_{d5}+residual \tag{4}$$

Here dz is the height step for a given model level, ρ_d the density of dry air, $\rho_v=\rho_d{\cdot}q_v$ the density of water vapor and $\rho_H=\rho_d{\cdot}q_H$ the density of hydrometeors. Equations (3) and (4) have been obtained after multiplying the right hand side terms of equations (1) and (2) by $dz{\cdot}\rho_d/\mu$, and replacing the left hand side terms, i.e., the tendency of $\mu{\cdot}q_v$ and $\mu{\cdot}q_H$, by the tendency of $dz{\cdot}\rho_v$ and $dz{\cdot}\rho_H$, respectively. Formally there appear additional tendencies in the left hand side terms of equations (3) and (4), i.e.,

$$dz\cdot\rho_v\cdot\left[\mu^{-1}\cdot(\mu)_t+{\rho_d}^{-1}\cdot(\rho_d)_t\right]$$

and

$$dz\cdot\rho_H\cdot\left[\mu^{-1}\cdot(\mu)_t+{\rho_d}^{-1}\cdot(\rho_d)_t\right],$$

respectively, which have been neglected. Also, the right hand side terms of equations (3) and (4) have been rearranged in order to express the tendency (c1, d1) as the sum of horizontal transport (c2, d2), vertical transport (c3, d3), phase change (c4, d4), and hydrometeors fallout (d5). A residual term appears in equations (3) and (4) since these equations are not strictly equivalent to equations (1) and (2), respectively, and therefore not exactly closed in the WRF model. Terms of equations (3) and (4) are integrated online at the time step of the model to provide a budget of atmospheric water vapor and hydrometeors.

3.2. Bulk Atmospheric Moisture Budget and Bulk Precipitation Recycling Ratio

Summing vertically the terms of equations (3) and (4) provides a budget comparable to that in *Schär et al*. [1999]. The grid-resolved horizontal transport terms in equations (3) and (4) are additionally decomposed in west, east, south and north flux components, and integrated online with the other terms, in order to extract the in- and outflow of atmospheric moisture. Considering a given domain (in our case domain δ or Δ), temporal variation of domain-averaged column-integrated atmospheric moisture W (deduced from the tendency terms in equations (3) and (4)) can be compared with the sum of inflow I and outflow O of atmospheric moisture (deduced from the decomposition of the grid-resolved horizontal transport terms in equations (3) and (4)), evaporation E and precipitation P within the domain, as

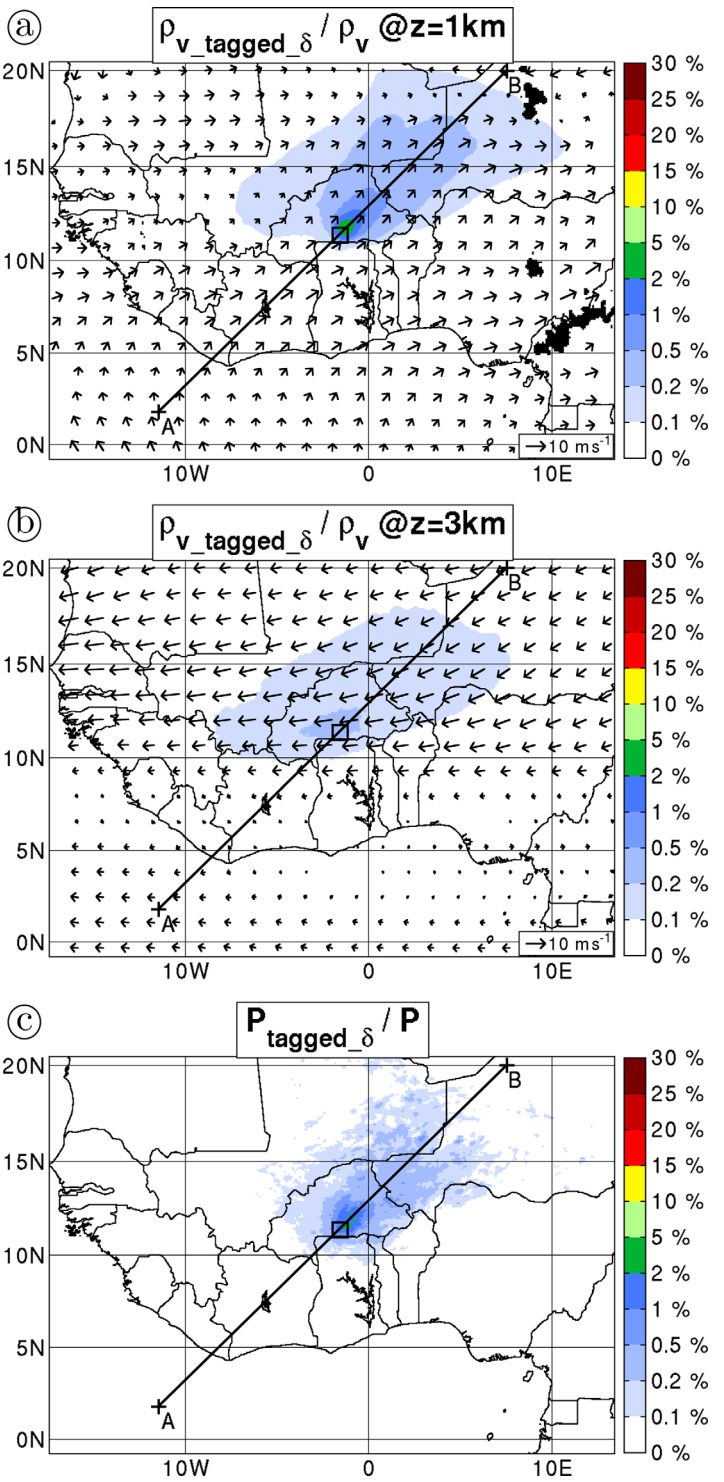

Figure 3. (a) Horizontal cross section at 1 km altitude of the WRF-derived ratio between the density of tagged water vapor originating from E in domain δ, i.e., $\rho_{v\_tagged\_\delta}$, and the density of total water vapor ρ_v in % (colour) and horizontal winds in m s^{-1} (arrows) averaged between 1 July and 31 August 2003. The scale of $\rho_{v\_tagged\_\delta}/\rho_v$ is given by the coloured bar on the right side and the wind scale by the arrow on the bottom right corner of the panel. The black square shows the location of domain δ. The straight black line (A-B) gives the location of the vertical cross sections in Figure 4. (b) As in Figure 3a, except at 3 km altitude. (c) As in Figure 3a, except for the ratio between tagged precipitation originating from E in domain δ, i.e., P_{tagged_δ}, and total precipitation P.

$$\frac{dW}{dt} = I - O + E - P + residual \quad (5)$$

A residual term also appears in equation (5) since this equation is not strictly verified in the WRF model (recalling equation (5) is derived from equations (3) and (4) which are also not strictly verified in the WRF model). Assuming (1) there is no return flow of atmospheric moisture originating from E inside the domain, and (2) the two atmospheric water fractions originating from E inside and outside of the domain are well mixed in the vertical [*Schär et al.*, 1999], a so-called bulk precipitation recycling ratio β_{bulk} can be written as

$$\beta_{bulk} = \frac{E}{E+I} \quad (6)$$

It is emphasized that sources of errors in this online bulk method are restricted to the two assumptions of no return flow and well vertical mixing, and the residual term in equation (5). In the traditional offline bulk method [e.g., *Schär et al.*, 1999] the coarse temporal resolution for the computation of the budget is an additional source of error in the evaluation of β_{bulk}.

3.3. Evaporation Tagging and Tagged Precipitation Recycling Ratio

E-tagging was firstly implemented in a regional atmospheric model by *Sodemann et al.* [2009]. Their procedure consisted in (1) initializing regions of tagged evaporated water, i.e., setting E_{tagged} equal to E inside the source region and zero outside, (2) applying the advection scheme on the tagged water species, these last ones being set to zero at the lateral boundaries of the model domain (no inflow of tagged

water species), and (3) computing tagged water phase changes as

$$C_{\alpha\rightarrow\beta,tagged}=C_{\alpha\rightarrow\beta}\frac{q_{\alpha,tagged}}{q_{\alpha}} \tag{7}$$

where $q_{\alpha,tagged}/q_{\alpha}$ is the fraction of tagged mass in the reservoir α (water vapor, liquid or solid water species), $C_{\alpha\rightarrow\beta}$ the mass transfer from reservoir α to reservoir β, and $C_{\alpha\rightarrow,tagged}$ the tagged mass flux. *Sodemann et al*. [2009] also added the following condition to avoid susceptible numerical errors in the advection scheme due to high tagged water gradients.

$$0\leq\frac{q_{\alpha,tagged}}{q_{\alpha}}\leq 1 \tag{8}$$

Knoche and Kunstmann [2013] elaborated a similar *E*-tagging method in MM5. In their case water phase changes of tagged water species were implemented in the Mixed-Phase scheme from *Reisner et al*. [1998]. As our WRF setup uses a similar microphysical scheme [i.e., *Hong et al*., 2004], it was straightforward to transfer the MM5 *E*-tagging method to our case. Also, in our WRF setup the *E* source of tagged water species from a predefined source area (in our case domain δ or Δ, see Figure 1) is implemented in the subgrid vertical transport scheme of *Hong et al*. [2006] (term F_{qv}^{V} in equation (1)).

Tagged water species, namely q_{v_tagged}, q_{c_tagged}, q_{r_tagged}, q_{i_tagged}, q_{s_tagged}, verifying similar prognostic equations as q_v, q_c, q_r, q_i and q_s, a version of equations (3) and (4), replacing ρ_v and ρ_H by $\rho_{v\_tagged}=\rho_d q_{v\_tagged}$ and $\rho_{H\_tagged}=\rho_d(q_{c\_tagged}+q_{r\_tagged}+q_{i\_tagged}+q_{s\ d\_tagged})$, respectively, are implemented in the code. In order to compare tagging results with that of the bulk method presented in section 3.2, we define the so-called tagged precipitation ratio β_{tagged} as

$$\beta_{tagged}=\frac{P_{tagged}}{P} \tag{9}$$

In the following, variables associated with water species originating from *E* in domain δ (Δ), have the subscript tagged_δ(Δ).

3.4. About the Validity of the Bulk Method

Recalling that E_{tagged} is equal to *E* in the source region of tagged water species (in our case domain δ or Δ) and zero outside, the bulk budget equation of tagged atmospheric moisture for this region can be written as

$$\frac{dW_{tagged}}{dt}=I_{tagged}-O_{tagged}+E-P_{tagged}+residual \tag{10}$$

In equation (10), W_{tagged}, I_{tagged}, O_{tagged} and P_{tagged} give the contribution of tagged water species to the terms *W*, *I*, *O* and *P* of equation (5), respectively. In case of no return flow, I_{tagged} is equal to zero [e.g., *Schär et al*., 1999], whereas in case of well vertical mixing between total and tagged water species the ratios

$$\beta_W=\frac{dW_{tagged}}{dW},$$

$$\beta_O=\frac{O_{tagged}}{O}$$

and

$$\beta_{tagged}=\frac{P_{tagged}}{P}$$

are identical [e.g., *Eltahir and Bras*, 1996]. In this particular case, β_{tagged} is equal to $\beta_{bulk}=E/(E+I)$. In the general case, defining

$$\beta_I=\frac{I_{tagged}}{I},$$

we find that

$$\beta_{tagged} = \beta_{bulk} + \underbrace{\beta_I \cdot \left(\frac{I}{E+I}\right)}_{\varepsilon_I} + \underbrace{\left(\beta_{tagged} - \beta_O\right) \cdot \left(\frac{O}{E+I}\right)}_{\varepsilon_O} + \underbrace{\left(\beta_{tagged} - \beta_W\right) \cdot \left(\frac{dW/dt}{E+I}\right)}_{\varepsilon_W} + residual \quad (11)$$

In equation (11), β_{tagged} is the sum of β_{bulk} and three additional terms related to return flow (ε_I) and nonwell vertical mixing of the outflow and atmospheric moisture in the source region (ε_O and ε_W, respectively). As in equations (5) and (10), a residual term also appears in equation (11) since this equation is not strictly verified in the WRF model (recalling equation (11) is derived from equations (3) and (4) which are also not strictly verified in the WRF model). Equation (11) allows quantifying the contribution of return flow and nonwell vertical mixing to regional precipitation recycling, which is neglected in the bulk method.

4. Regional Precipitation Recycling Analysis at the 100 × 100 km^2 Scale

4.1. Qualitative Analysis

Regional precipitation recycling mechanisms in the 100 × 100 km^2 domain δ (see Figure 1) are investigated with the WRF simulation using domain δ as source region for *E*-tagging. Figures 3a and 3b display the ratio $\rho_{v\_tagged\_\delta}/\rho_v$ at 1 and 3 km altitude, respectively, averaged for a 2 month period during the wet season, i.e., July–August 2003. During this period, domain δ is characterized by southwesterlies in the low levels and easterlies in the mid-levels, as in the case of *Knoche and Kunstmann* [2013]. Accordingly, the ratio $\rho_{v\_tagged\_\delta}/\rho_v$ is maximum to the Northeast (West) of domain δ at 1 (3) km altitude (Figures 3a and 3b). As a consequence of this vertical wind shear condition, tagged precipitation in July–August 2003 is largely falling outside of domain δ to the Northeast, slightly southwest of the maximum of $\rho_{v\_tagged\_\delta}/\rho_v$ at 1 km altitude (compare Figures 3a and 3c). Similar results have been obtained for the other months of the wet season during April–October (not shown). In March, $\rho_{v\_tagged\_\delta}/\rho_v$ at 1 km altitude displayed a maximum southwest of domain δ, in association with low-level northeasterly wind conditions prevailing at this time (not shown).

An example of convective transport of tagged water vapor from the source region in the low levels to the mid- and upper troposphere is given in Figure 4. This figure displays vertical cross sections, along the line (A-B) shown in Figure 3, of $\rho_{v\_tagged\_\delta}/\rho_v$ and winds projected on the plan of the cross section for a 24 h period from 7 July 2003 09 UTC. Evaporated water from domain δ is lifted up to 3 km at 15 UTC (Figures 4a–4c). During the afternoon, convection in the vicinity of domain δ lifts tagged water vapor up to 14 km altitude (Figures 4d–4f). The vertical column of tagged water vapor is subsequently sheared in association with the wind shear condition occurring at that time (Figures 4g–4h). Such vertical lifting and shearing occurs at a frequency of 1–4 days (see supporting information movie file displaying vertical cross sections of Figure 4 for the period July–August 2003).

4.2. Budget Analysis

Regional precipitation recycling mechanisms in domain δ are quantified with the methods of section 3. In particular, terms of the budgets of ρ_v and ρ_H from equations (3) and (4), respectively, are averaged horizontally in domain δ and visualized as 3 hourly time-height profiles for 1–10 July 2003 in Figures 5a–5d and Figures 6a–6e, respectively. The contribution of tagged water species originating from *E* in domain δ, i.e., $\rho_{v\_tagged\_\delta}$ and $\rho_{H\_tagged\_\delta}$, respectively, to the terms of the above budgets is shown in Figures 5e–5h and Figures 6f–6j, respectively. The residual terms in these budgets are one to three orders of magnitude below the terms displayed (not shown). The 10 day period 1–10 July has been chosen as a compromise between the amount of data visualized and the readability of the results at the 3 hourly scale. Comparable results have been obtained for the whole simulated wet season.

Terms in the budget of *W* (equation (6)) in domain δ are visualized as daily time series in Figure 7a for the period March–October 2003. The contribution of $\rho_{v\_tagged\_\delta}$ and $\rho_{H\_tagged\_\delta}$ to these terms (equation (10)) is shown in Figure 7b. The residual terms in the budgets are also relatively small compared to the other terms (see thick black lines in Figure 7). Daily and monthly time series of tagged and bulk precipitation recycling ratios in domain δ, β_{bulk_δ} (equation (6)) and β_{tagged_δ} (equation (9)), respectively, as well as the additional terms in equation (11) quantifying the effect of return flow (ε_I) and nonwell vertical mixing (ε_O and ε_W), are

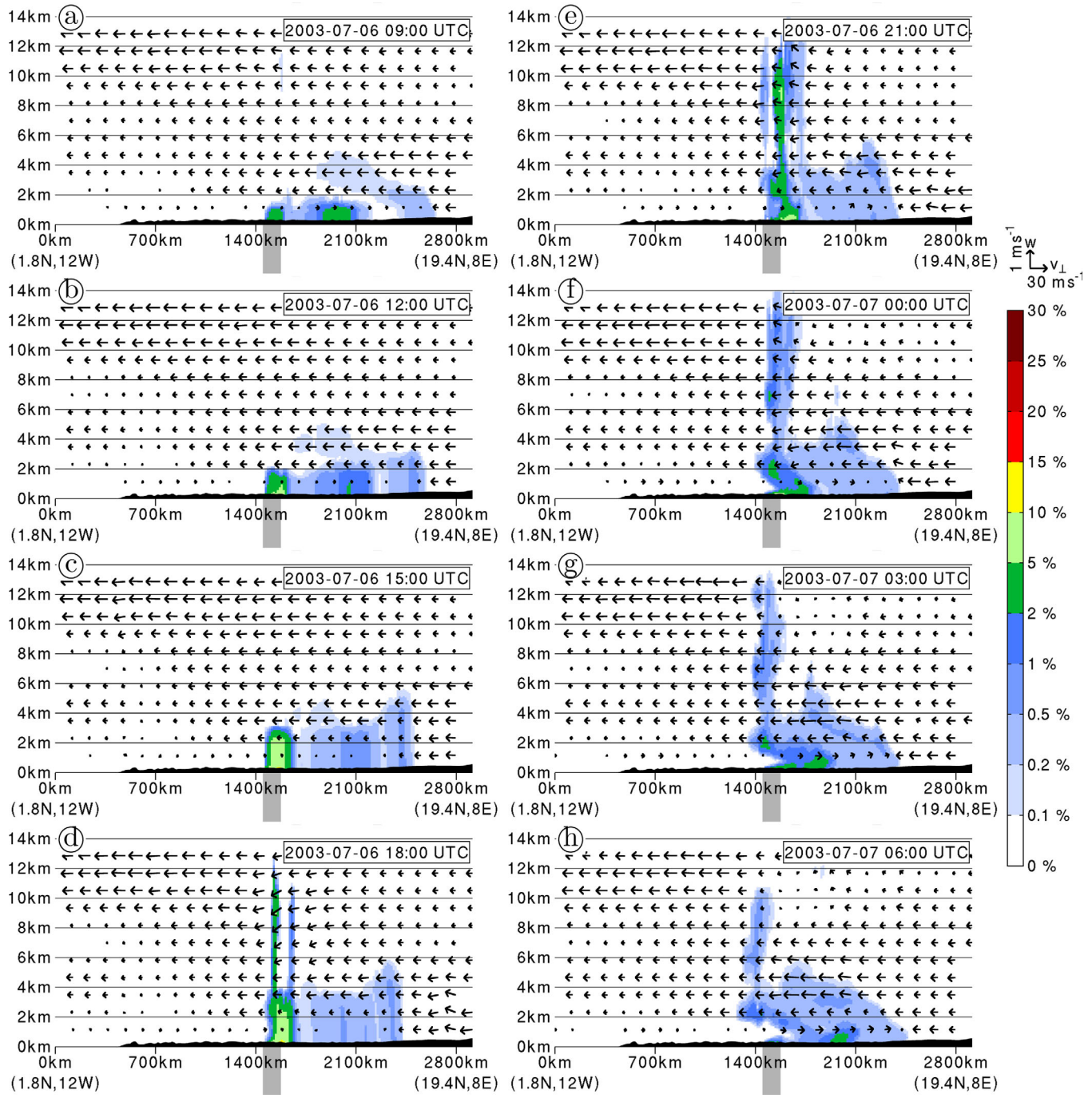

Figure 4. (a) Vertical cross section of the WRF-derived ratio between the density of tagged water vapor originating from E in domain δ, i.e., $\rho_{v\_tagged\_\delta}$, and the density of total water vapor ρ_v in % (colour) and winds projected on the plan of the cross section in m s^{-1} (arrows), at the location indicated by line (A-B) in Figure 3 and at 09 UTC 1 August 2003. The horizontal axis gives the horizontal coordinate in km and the vertical axis gives the altitude in km. The grey shade below the horizontal axis gives the location of domain δ. The profile of the West African continent is shaded in black. The scale of $\rho_{v\_tagged\_\delta}/\rho_v$ is given by the coloured bar on the right side of the panel. The projected winds take into account the vertical velocity and the scale is given by the arrows on the top right corner of the plot. (b–f) As in Figure 4a, except for consecutive times at a 3 h interval.

provided in Figure 8. The total contribution of these terms for the period March–October 2003 is given in Table 2.

4.2.1. Water vapor and hydrometeors budget results

The time-height profiles of the tendencies of ρ_v and ρ_H are characterized by elongated vertical strips of positive and negative values in the whole troposphere, with a period of oscillation of 1–3 days (Figures 5a and 6a). This is the signature of modeled deep convective events occurring in domain δ.

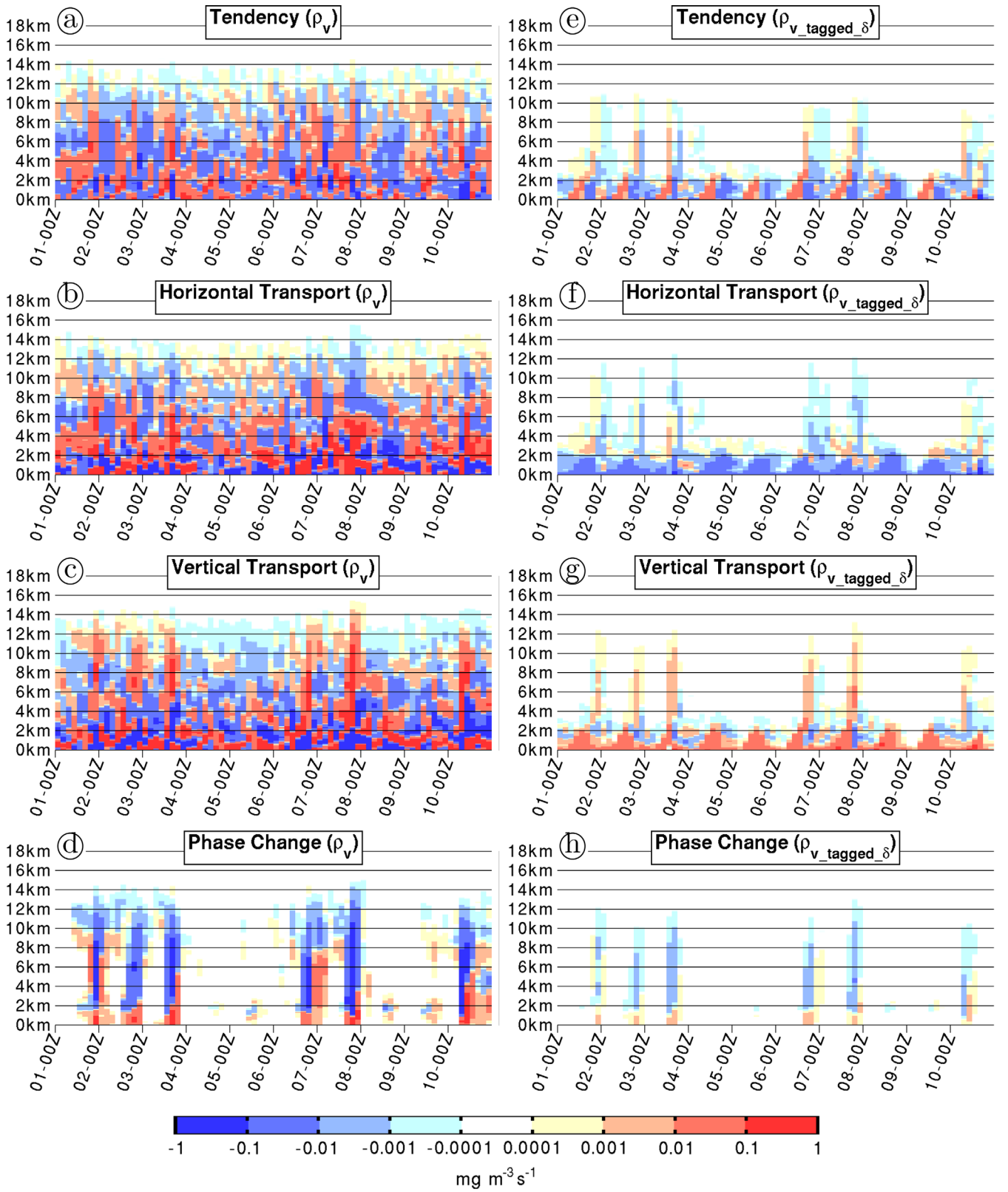

Figure 5. (a–d) WRF-derived time-height diagrams of the terms of the daily budget of the density of water vapor ρ_v (obtained by dividing equation (3) by *dz*) spatially averaged in domain δ: (a) tendency, (b) horizontal transport, (c) vertical transport, (d) phase change. The x- and y axis give the time from 00 UTC 1 July to 00 UTC 11 July 2003, and the average height above the surface, respectively. (e-h) As in the left column, except for the terms of the budget of the density of tagged water vapour originating from *E* in domain δ, i.e., $\rho_{v\_tagged\_\delta}$, spatially averaged in domain δ. The tendency scale (mg m^{-3} s^{-1}) is the same for all panels and is given by the coloured bar at the bottom of the figure.

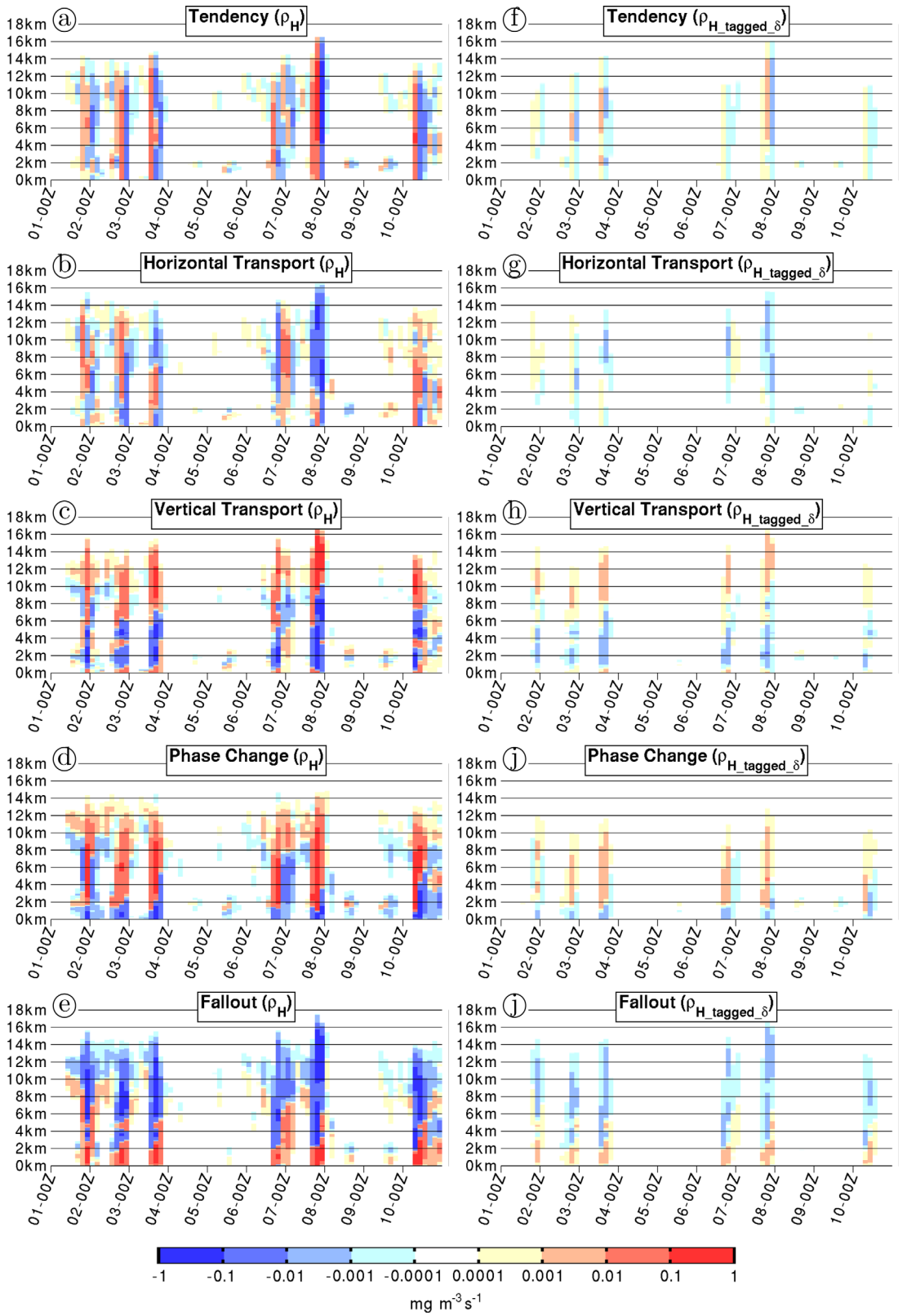

Figure 6. As in Figure 5, except for (a–e) the budget of the density of hydrometeors ρ_H and (f–j) the density of tagged hydrometeors originating from E in domain δ, i.e., $\rho_{H\_tagged\_\delta}$ (obtained by dividing equation (4) by dz), spatially averaged in domain δ.

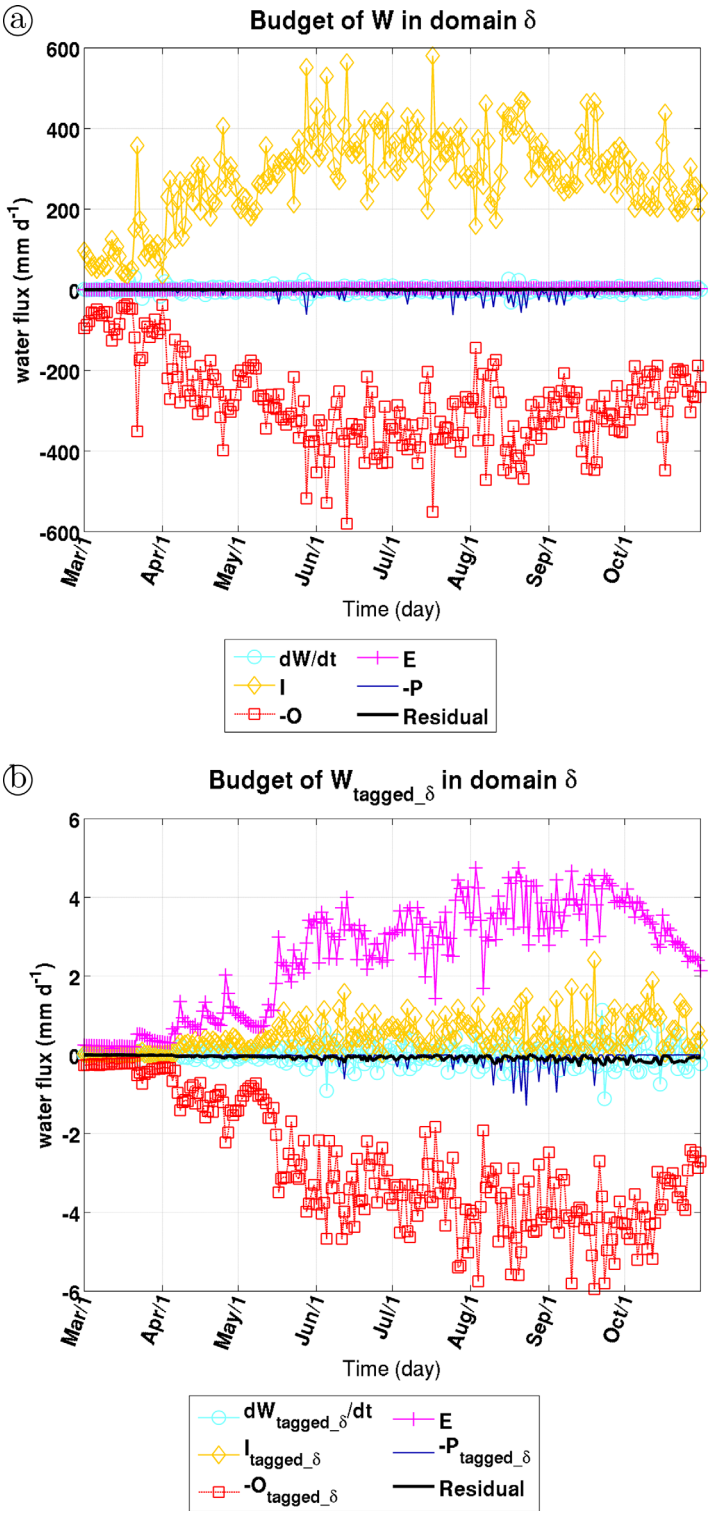

Figure 7. (a) WRF-derived daily time series of the terms of the budget of vertically-integrated atmospheric water W spatially averaged in domain δ (equation (5)). The x axis gives the time in days from March to October 2003, and the y axis the water amount in mm. (b) As in Figure 7a, except for the budget of vertically-integrated tagged atmospheric water originating from E in domain δ, i.e., W_{tagged_δ}, spatially averaged in domain δ (equation (10)).

In the budget of ρ_v (Figures 5a–5d), the production of ρ_H (destruction of ρ_v) through water phase changes mainly occurs above 2 km during these deep convective events, as shown by the elongated vertical strips of negative values in the phase change term (Figure 5d). These negative elongated vertical strips are counterbalanced by positive and negative values in the tendency term (compare Figure 5a and Figure 5d), positive values in the horizontal transport term up to 6–10 km, negative above (compare Figure 5b and Figure 5d), and positive values in the vertical transport term above 2 km (compare Figure 5c and Figure 5d). This is coherent with the fact that deep convective updrafts are expected to transport ρ_v from mid- to upper levels, while convectively-enhanced low to mid-level (mid- to upper level) convergence (divergence) is expected to partly sustain (hinder) the accumulation of ρ_v in the mid- to upper levels, resulting in temporal oscillations of ρ_v.

In the budget of ρ_H (Figures 6a–6e), the hydrometeors fallout term is generally negative (positive) in the mid-upper troposphere (lower troposphere) (see Figure 6e). Positive fallout in the lower troposphere is related to a loss of ρ_H through phase change (compare Figures 5d and 6d below 2 km), so that more precipitation enters the low levels than actually reaches the surface. Negative fallout in the mid-upper troposphere is then related to the production of ρ_H through condensation/deposition at these heights (see Figures 5d and 6d above 2 km), so that in each layer of the mid-upper troposphere there is always more ρ_H precipitating at

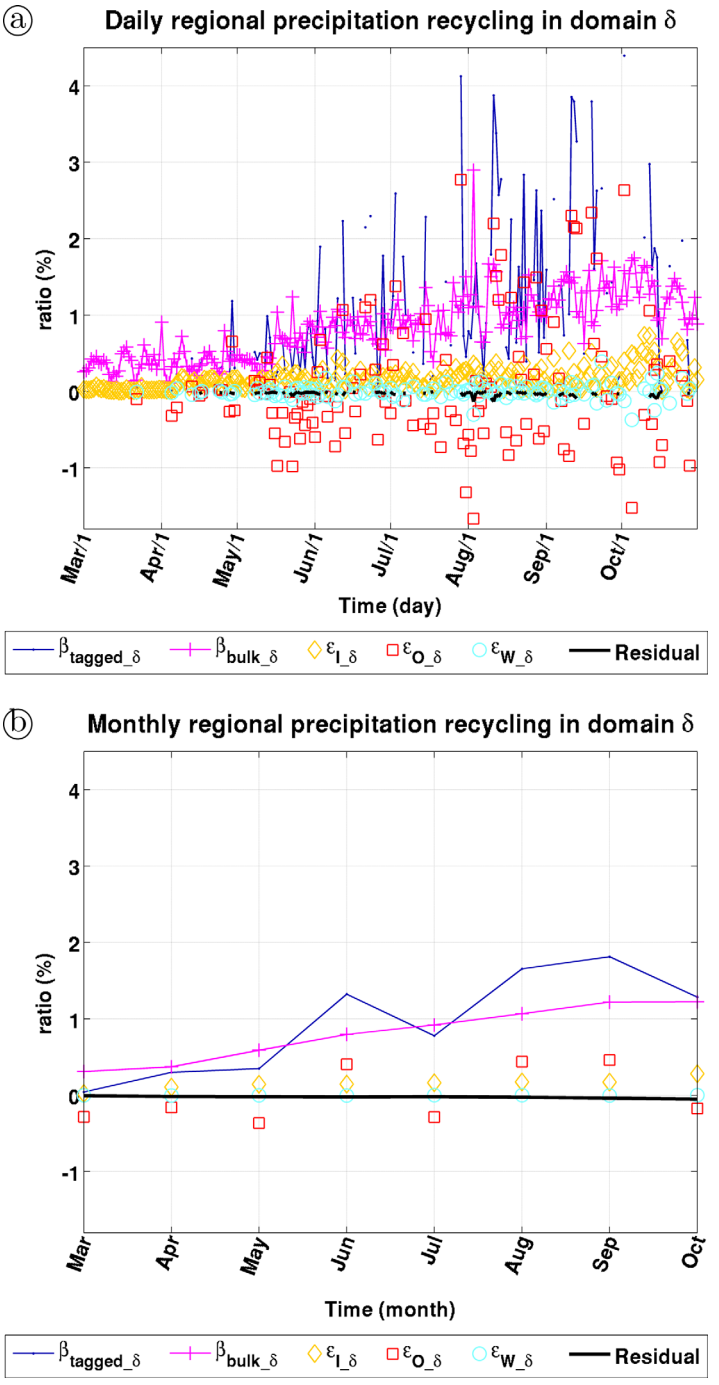

Figure 8. (a) WRF-derived daily time series of the terms of equation (11) averaged in domain δ, i.e., the tagged precipitation ratio β_{tagged_δ}, the bulk precipitation ratio β_{bulk_δ}, the three additional terms quantifying the contribution of return flow (ε_{I_δ}) and nonwell vertical mixing (ε_{O_δ} and ε_{W_δ}) to regional precipitation recycling in domain δ, and a residual term. Values of β_{tagged_δ}, ε_{O_δ}, ε_{W_δ} and residual term are displayed only for daily precipitation greater than 0.1 mm d^{-1}. The x axis gives the time in days from March to October 2003, and the y axis the precipitation recycling ratio in %. (b) As in Figure 8a, except monthly.

the bottom than at the top of the considered layer. There is also an accumulation (dispersion) of ρ_H by vertical transport above (below) 8 km shown in Figure 6c, as deep convective updrafts displace ρ_H from mid- to upper levels, which significantly contributes to the hydrometeors fallout mechanism. The horizontal transport term has a comparable contribution in the budget of ρ_H (see Figure 6b). Also, this horizontal transport occurs in both directions between the inside and outside of domain δ, depending on time and height, so that the production and fallout of hydrometeors in this simulated West African atmosphere is not strictly a local process at the 100 × 100 km^2 scale.

The budget of W in domain δ (see Figure 7a) is largely dominated by the in- and outflow terms. Accordingly, the contribution of E in this budget is almost negligible (see magenta line with plus signs in Figure 7a), leading to a β_{bulk_δ} of about 0.9% for the simulated period March–October 2003 (see Figure 8 and Table 2). Interestingly, there is a general increase of β_{bulk_δ} with respect to time for the whole considered period, especially at the monthly scale (see Figure 8b), in association with wetter soils and higher E at the end of the wet season (see magenta line with plus signs in Figure 7b).

4.2.2. Tagged Water Vapor and Hydrometeors Budget Results

According to the budget of $\rho_{v\_tagged\_\delta}$ (Figures 5e–5g), evaporated water from domain δ is for a larger part transported laterally outside of domain δ in the low levels (see negative values below 2 km in Figure 5f), and for a smaller part transported upward up to the mid-levels (see elongated vertical strips of positive values up to 10 km in Figure 5g). The fact that the horizontal transport term (Figure 5f) is mainly negative through the whole troposphere further confirms

Table 2. As in Table 1, Except for the Terms of Equation (11) (First Column) Computed for the Period March–October 2003 for Domain δ (Second Column) and for Domain Δ (Third Column)[a]

	Domain δ	Domain Δ
β_{tagged}	1.23%	11.83%
β_{bulk}	**0.87%** (71%)	**7.33%** (61.9%)
ε_I	**0.16%** (13.2%)	**2.94%** (24.8%)
ε_O	**0.22%** (17.9%)	**1.61%** (13.6%)
ε_W	**0%** (0%)	**−0.02%** (−0.2%)
Residual	**−0.03%** (−2.1%)	**−0.02%** (−0.1%)

[a]The contribution of β_{bulk}, ε_I, ε_O, ε_W and a residual term to the tagged precipitation recycling ratio β_{tagged} is given in absolute value (in bold) and in relative value (in parenthesis).

that mid-upper tropospheric $\rho_{v\_tagged\_\delta}$ mainly originates from convective lifting inside domain δ. Weak positive values in this horizontal transport term at 2–6 km still suggest that a small part of tagged water does return in domain δ in the mid-levels after convective lifting outside of domain δ, such as in the atmospheric water pathway from *Knoche and Kunstmann* [2013] (see section 4.1, Figures 3a and 3b, Figure 4). The contribution of $\rho_{v\_tagged\_\delta}$ to the mid-upper tropospheric production and fallout of hydrometeors is accordingly small (compare Figure 5d and Figure 5h, Figures 6c–6e and Figures 6h–6j).

A β_{tagged_δ} of about 1.2% is obtained for the simulated period March–October 2003 (see Figure 8), which is slightly higher than the 0.9% obtained for β_{bulk_δ} (Table 2). There is indeed a small inflow of tagged water (tagged water leaving the domain and coming back, see yellow solid line with diamonds in Figure 7b), so that the assumption of no return flow from *Schär et al.* [1999] is not strictly verified in this case. At the monthly scale, β_{tagged_δ} is characterized by larger time fluctuations in comparison to β_{bulk_δ} (Figure 8b). For August 2003, β_{tagged_δ} is about 1.7%, while β_{bulk_δ} is about 1.1%. Our tagging result is close to that of *Knoche and Kunstmann* [2013] who also obtained a β_{tagged} of 1.7% for a 160 × 250 km^2 source area in August 1998 (we recall that domain δ has an area of 100 × 100 km^2). At the daily scale, β_{tagged_δ} displays oscillations between 0 and 4% (see dark blue solid line in Figure 8a), with highest values reached in August–September. β_{bulk_δ} does not pick up these large daily variations (see magenta solid line with plus signs in Figure 8a). It is noted that the definition of β_{bulk_δ} can provide a daily precipitation recycling ratio even for days without rain.

To conclude this section, a prerequisite condition for evaporated water to participate to the precipitation process in domain δ is that it is first lifted to the mid-levels. In this case, however, this lifting mainly occurs on water vapor originating from *E* outside of domain δ.

4.2.3. Effect of Nonwell Vertical Mixing and Return Flow

Differences between β_{tagged_δ} and β_{bulk_δ} are related to the fact that the assumptions of no return flow and well-vertical mixing are not strictly verified, leading nonnegligible contribution of ε_{I_δ}, ε_{O_δ} and ε_{W_δ} in equation (11) at the daily and monthly scale (Figure 8), and for the period March–October 2003 (Table 2). The large daily variations in β_{tagged_δ} are mainly related to ε_{O_δ} (compare dark blue solid line and red squares in Figure 8a). The smaller contribution of ε_{W_δ} at the daily scale almost completely vanishes at the monthly scale (see light blue circles in Figures 8a and 8b). This is related to the fact that atmospheric moisture storage has a small but nonnegligible contribution in the atmospheric moisture budget in domain δ at the daily scale, and a negligible one at the monthly scale. ε_{I_δ} and ε_{O_δ} are small in March and increase significantly from April (see yellow diamonds and red squares in Figure 8), in coherence with the fact that vertical wind shear conditions in West Africa during the wet season, i.e., southwesterlies in the low levels and easterlies in the mid-levels, are in March not settled yet.

For the period March–October 2003, as shown in Table 2, the 1.2% of β_{tagged_δ} is distributed in 71% of β_{bulk_δ}, 13.2% of ε_{I_δ}, 17.9% of ε_{O_δ}, 0% of ε_{W_δ} and −2.1% of the residual term (see equation (11)). Assuming this residual term can be distributed to each of the right hand side terms in equation (11), the contribution of return flow and nonwell vertically mixed outflow to regional precipitation recycling in domain δ is about 13 and 17%, respectively.

5. Regional Precipitation Recycling Analysis at the 1000 × 1000 km^2 scale

5.1. Qualitative Analysis

Regional precipitation recycling mechanisms in the 1000 × 1000 km^2 domain Δ (see Figure 1) are investigated with the WRF simulation using domain Δ as source region for *E*-tagging. Figures 9a and 9b display the ratio $\rho_{v\_tagged\_\Delta}/\rho_v$ at 1 and 3 km altitude, respectively, averaged for July–August 2003. Figure 10

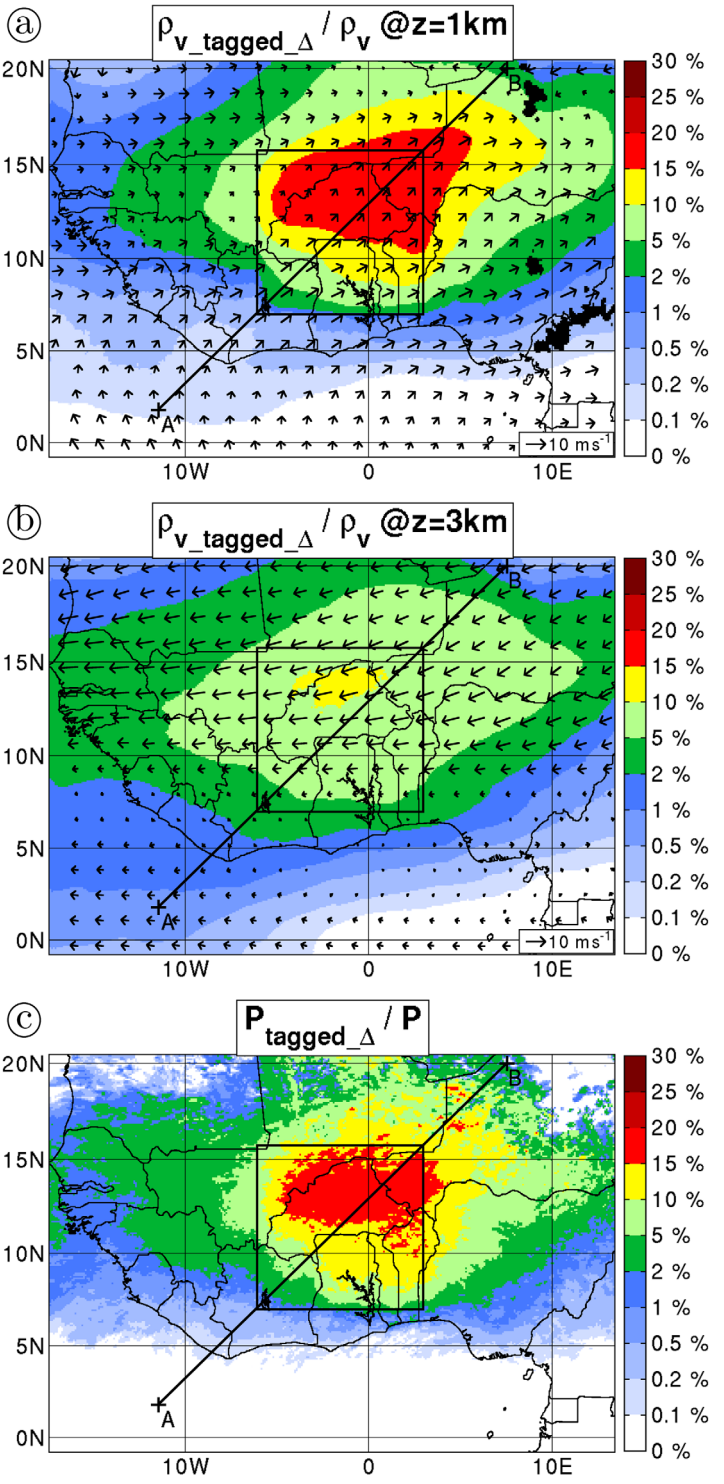

Figure 9. As in Figure 3, except for (a,b) the ratio between the density of tagged water vapor originating from E in domain Δ, i.e., $\rho_{v\_tagged\_\Delta}$, and the density of total water vapor ρ_v and (c) the ratio between the tagged precipitation originating from E in domain Δ, i.e., P_{tagged_Δ}, and total precipitation P. The black square shows the location of domain Δ.

displays vertical cross sections, along the line (A-B) shown in Figure 3, of $\rho_{v\_tagged\_\Delta}/\rho_v$ and winds projected on the plan of the cross section for a 24 h period from 7 July 2003 09 UTC. As tagged water vapor originating from E in domain δ, tagged water vapor originating from E in domain Δ is also transported northeastward in the low levels by the oceanic monsoon flow, and westward by the African Easterly Jet (AEJ) in the mid-levels (compare Figure 3a and Figure 9a, Figure 3b and Figure 9b, Figure 4 and Figure 10). Interestingly, the maxima of the ratio $\rho_{v\_tagged\_\Delta}/\rho_v$ ($\rho_{v\_tagged\_\delta}/\rho_v$) at 1 and 3 km altitude are located inside (outside) of the source region. Also, $\rho_{v\_tagged\_\Delta}/\rho_v$ is generally larger than $\rho_{v\_tagged\_\delta}/\rho_v$ and display significant values at higher altitudes and enhanced nonwell vertical mixing (compare Figure 4 and Figure 10). It is indeed found that convective lifting of water vapour evaporating from domain Δ occurs almost every day (see supporting information movie file displaying vertical cross sections of Figure 10 for the period July–August 2003). It is striking to see that even in the lowest levels above domain δ $\rho_{v\_tagged\_\delta}/\rho_v$ does not reach values as high as that reached by $\rho_{v\_tagged\_\Delta}/\rho_v$.

As a consequence of this scale effect, a larger (smaller) part of tagged precipitation from domain Δ (δ) is falling inside of the source region in July–August 2003 (compare Figure 3c and Figure 9c). Similar results have been obtained for the other months of the simulated wet season (not shown).

5.2. Budget Analysis

Regional precipitation recycling mechanisms in domain Δ are quantified with the methods of section 3. Note that the budget results for domain Δ, displayed in Figures 11–14 and Table 2, are visualized in the

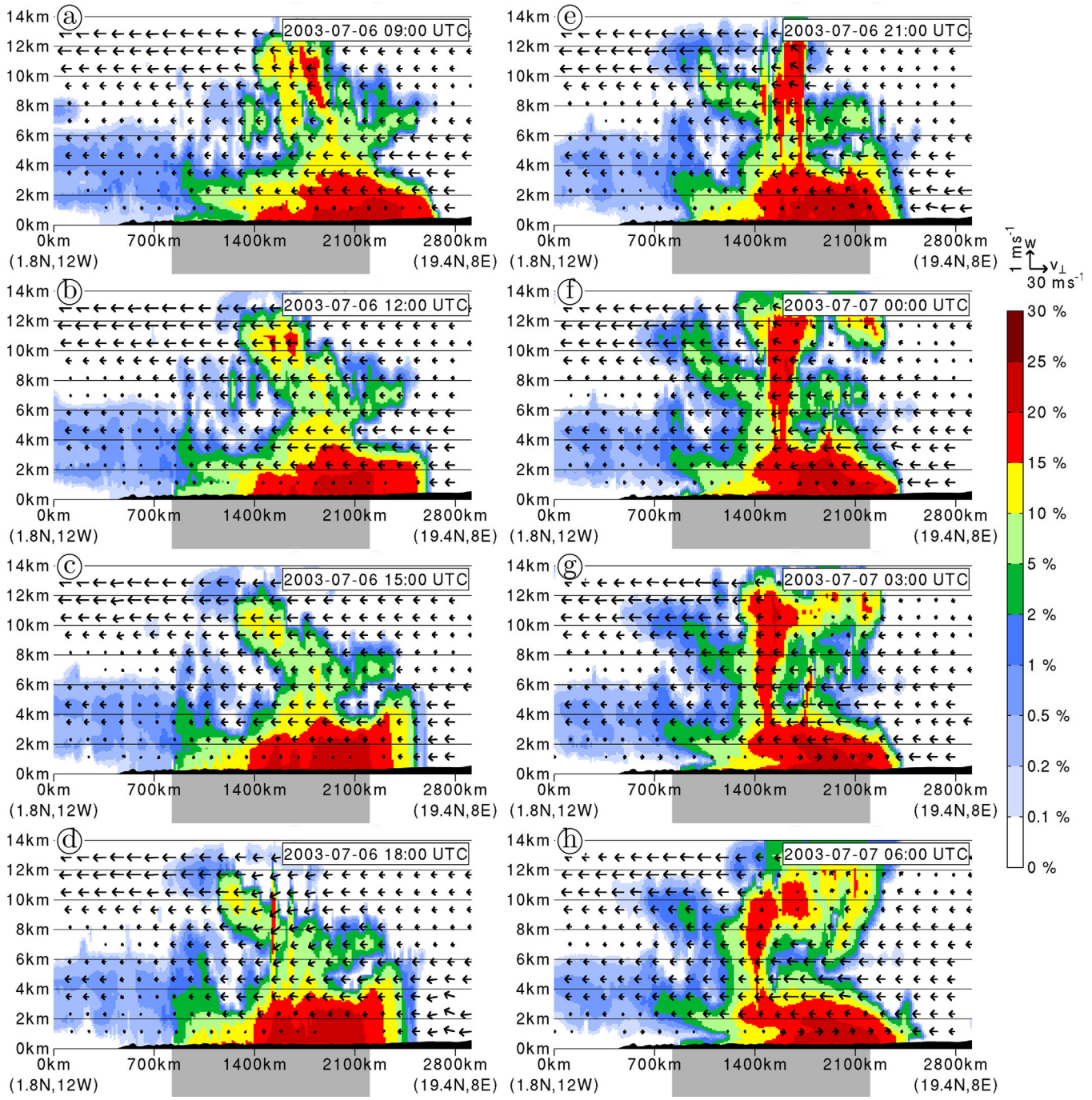

Figure 10. As in Figure 4, except for the ratio between the density of tagged water vapor originating from E in domain Δ, i.e., $\rho_{v\_tagged\_\Delta}$, and the density of total water vapor ρ_v. The grey shade below the horizontal axis gives the location of domain Δ.

same manner as those previously discussed for domain δ, displayed in Figures 5–8 and Table 2. As for the budgets in domain δ, the residual terms for the budgets in domain Δ are also small (partially shown).

5.2.1. Water Vapor and Hydrometeors Budget Results

One difference between the budgets in domains δ and Δ is the weaker amplitude of the elongated vertical strips in the time-height profiles of the tendency terms for domain Δ, suggesting that the spatial density of deep convective updrafts in domain Δ is less than in domain δ (compare Figure 5a and Figure 11a, Figure 6a and Figure 12a). Otherwise, the vertical profiles of the terms of the budgets of ρ_v and ρ_H in domain Δ

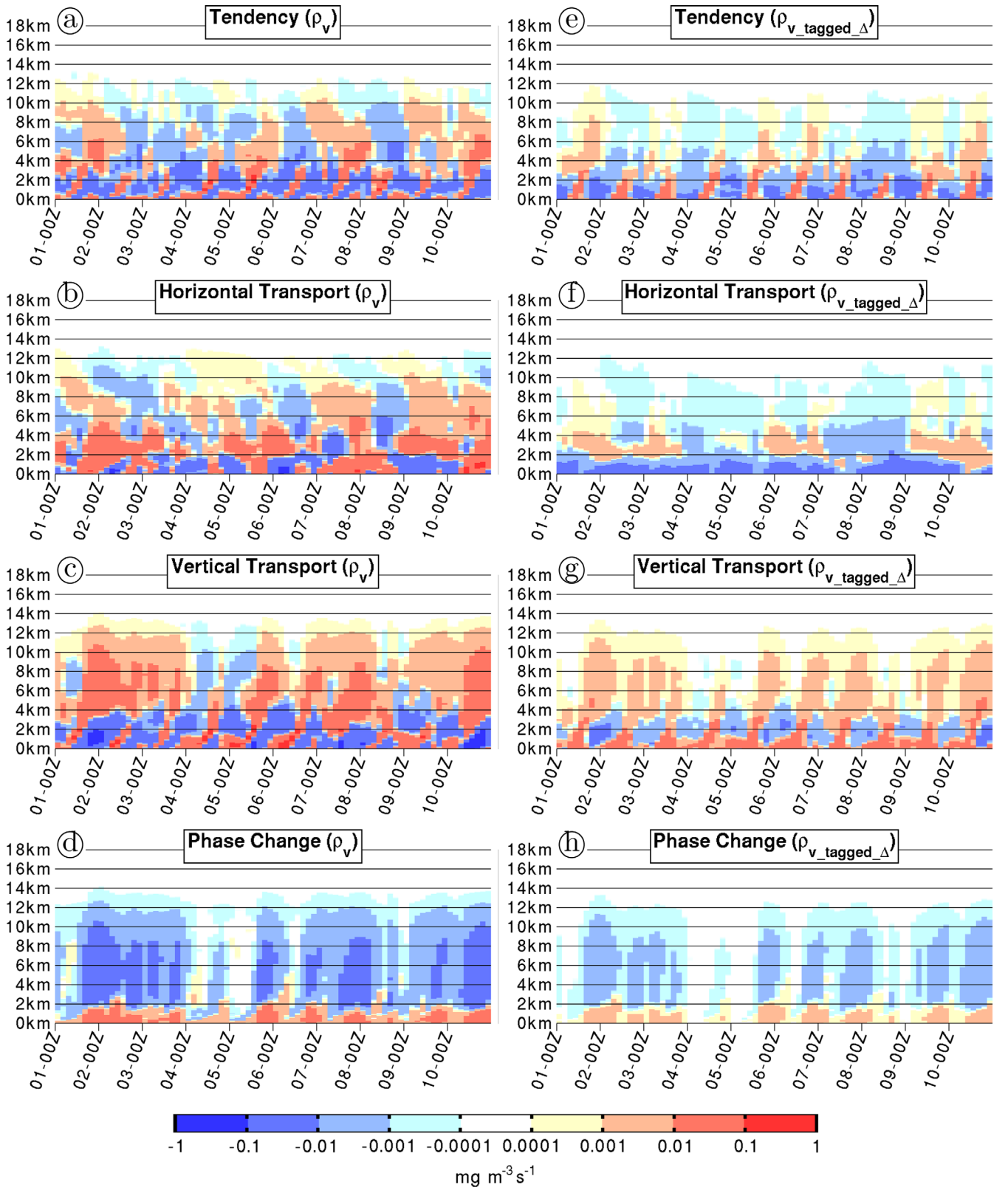

Figure 11. As in Figure 5, except for (a and b) the budget of the density of water vapor ρ_v and (e–h) the density of tagged water vapor originating from E in domain Δ, i.e., $\rho_{v\_tagged\_\Delta}$, spatially averaged in domain Δ.

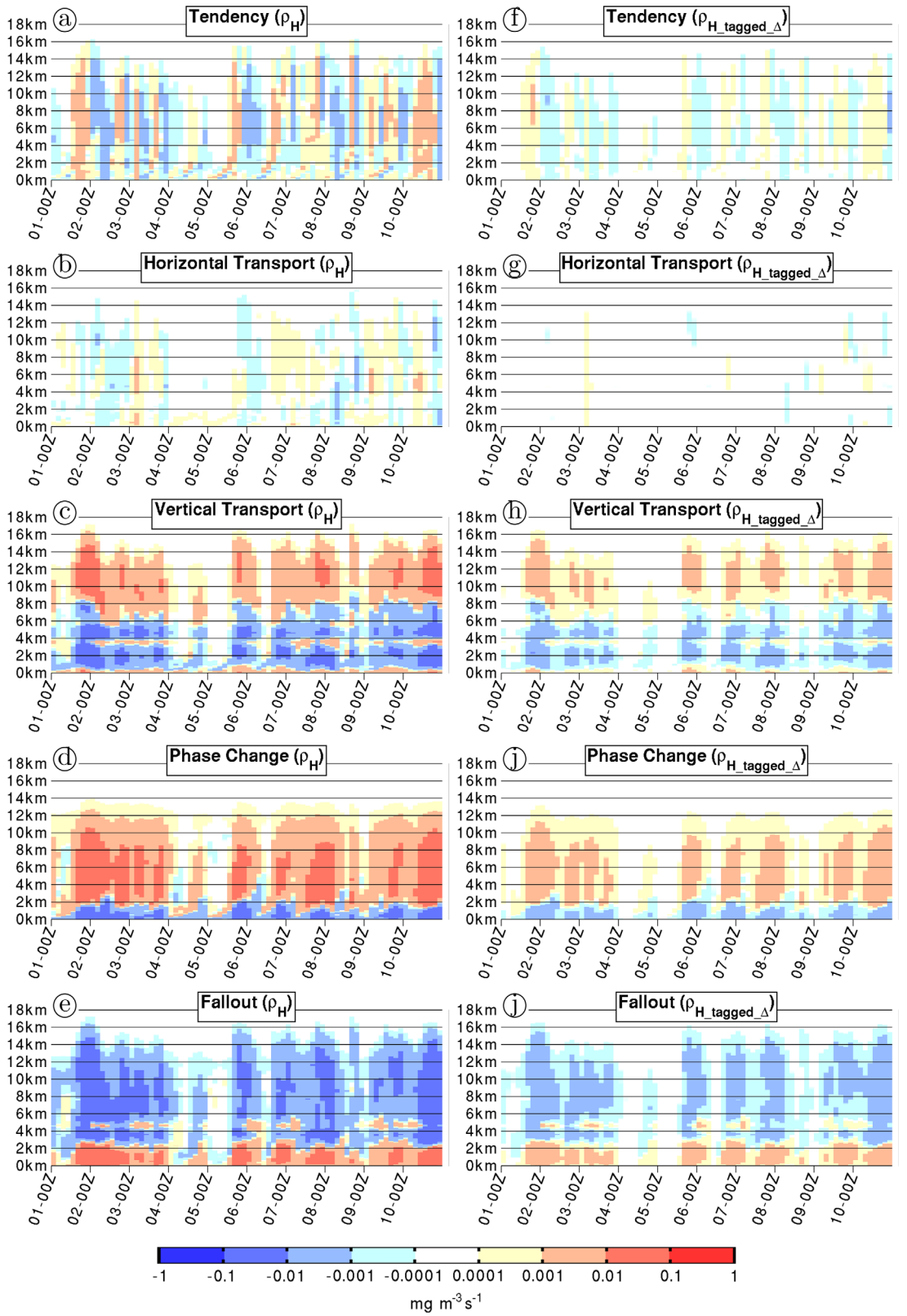

Figure 12. As in Figure 5, except for (a–e) the budget of the density of hydrometeors ρ_H and (f–j) the density of tagged hydrometeors originating from E in domain Δ, i.e., $\rho_{H\_tagged\_\Delta}$, spatially averaged in domain Δ.

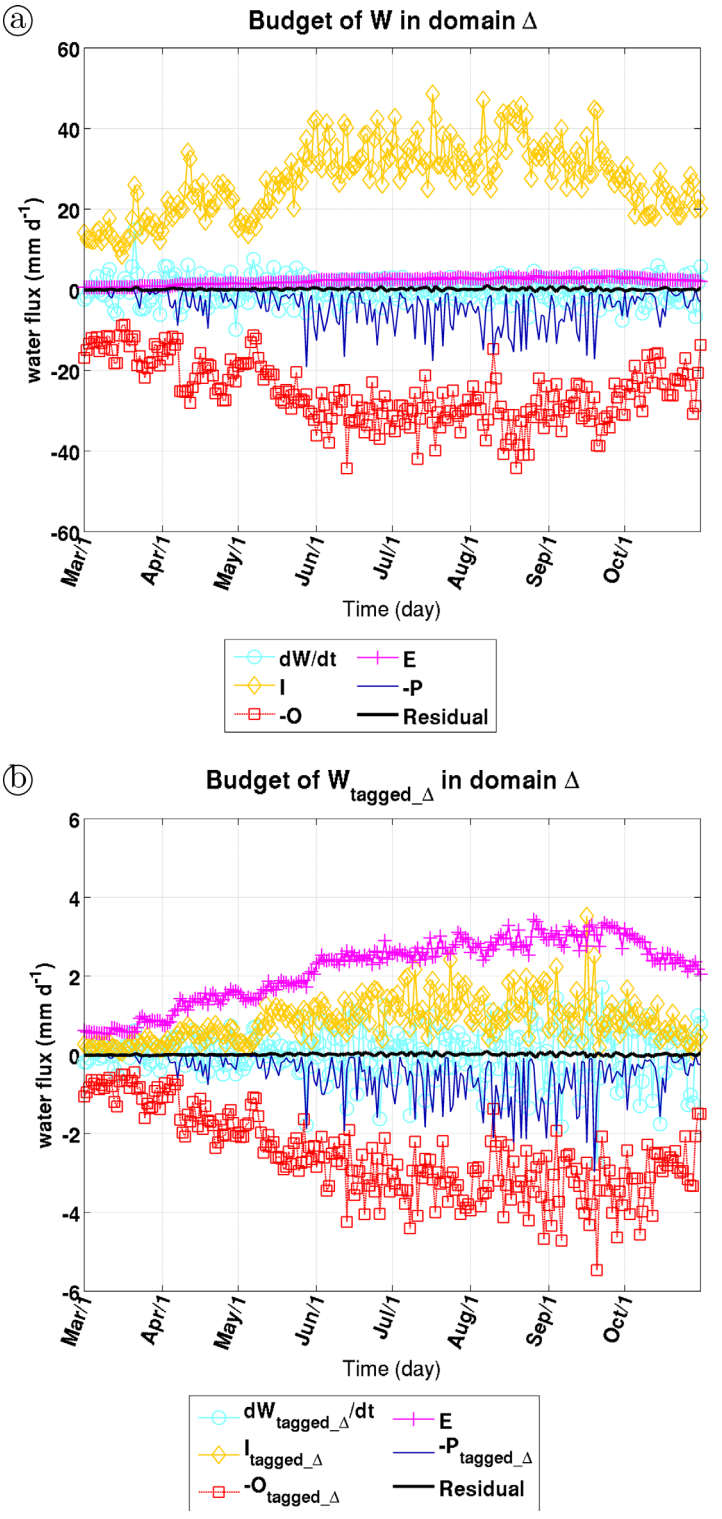

Figure 13. As in Figure 7, except (a) for the budget of vertically-integrated tagged atmospheric water W and (b) vertically-integrated tagged atmospheric water originating from E in domain Δ, i.e., W_{tagged_Δ}, spatially averaged in domain Δ.

display similar features as those in domain δ. In particular, the production of ρ_H (destruction of ρ_v) in the mid-upper troposphere through water phase changes (see negative values in Figure 11d) is also counterbalanced by positive and negative values in the tendency term (compare Figure 11a and Figure 11d), positive values in the horizontal transport term up to 6–10 km, negative above (compare Figure 11b and Figure 11d), and positive values in the vertical transport term above 2 km (compare Figure 11c and Figure 11d), in association with deep convective updrafts. Condensed/deposited particles are then mainly falling inside domain Δ with a negligible contribution of hydrometeors from outside domain Δ (see Figures 12a–12e), so that at the 1000 × 1000 km^2 scale the production and fallout of hydrometeors can be considered as a local process.

The budget of W (Figure 13) in domain Δ is less dominated by the in- and outflow terms as that in domain δ, these terms being generally one order of magnitude smaller in the case of domain Δ (compare Figure 7a and Figure 13a). Accordingly, the relative contribution of E in domain Δ is higher, leading to a β_{bulk_Δ} of about 7.3% for the simulated period March–October 2003 (see Figure 14 and Table 2). The fact that β_{bulk_Δ} is larger in domain Δ than in domain δ is a well-known scale effect [e.g., *Trenberth*, 1999, *Van der Ent and Savenije*, 2011]. Moreover, in domain Δ there is also a general increase of β_{bulk} with respect to time for the whole considered period, especially at the monthly scale (see Figure 14b), in association with wetter soils and higher E at the end of the wet season (see magenta line with plus signs in Figures 13a and 13b).

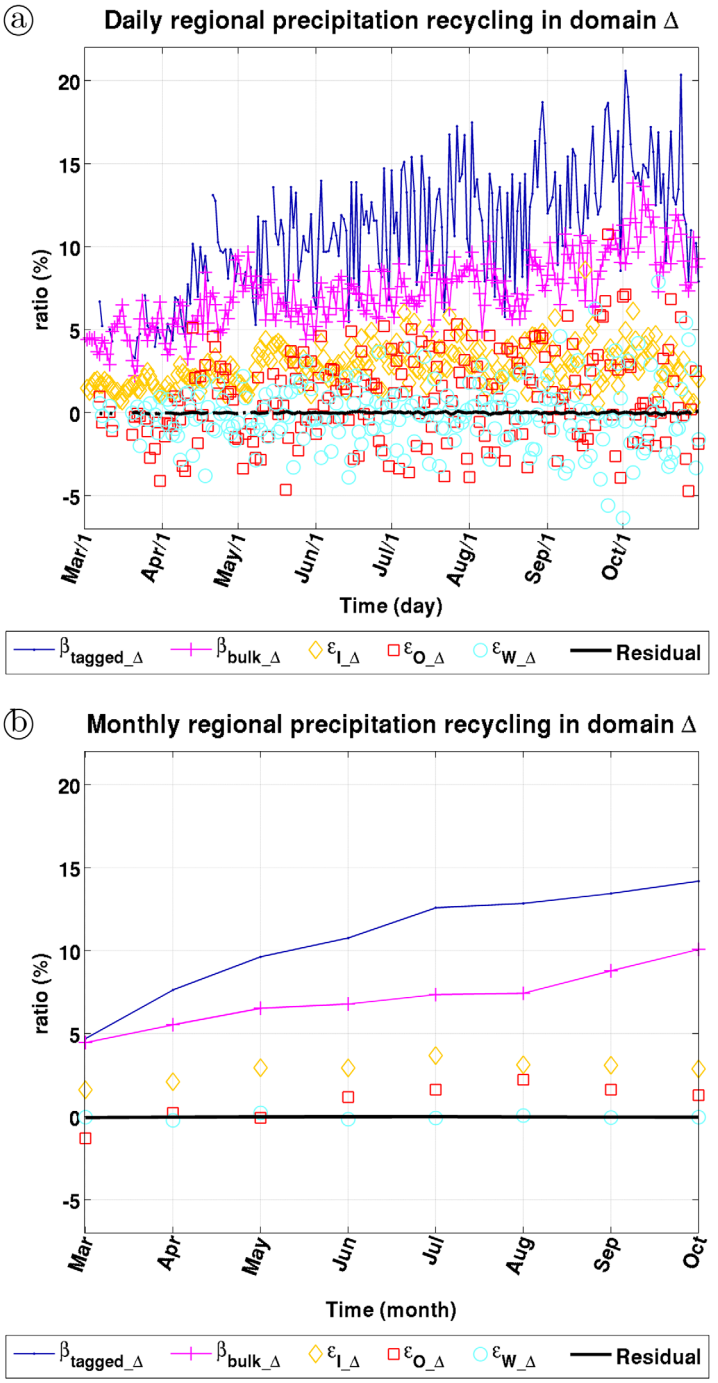

Figure 14. As in Figure 8, except for the terms of equation (11) averaged in domain Δ, i.e., the tagged precipitation ratio β_{tagged_Δ}, the bulk precipitation ratio β_{bulk_Δ}, the three additional terms quantifying the contribution of return flow (ε_{I_Δ}) and nonwell vertical mixing (ε_{O_Δ} and ε_{W_Δ}) on regional precipitation recycling in domain Δ, and a residual term.

5.2.2. Tagged Water Vapor and Hydrometeors Budget Results

The contribution of $\rho_{v\_tagged\_\Delta}$ and $\rho_{H\_tagged\_\Delta}$ to the terms of the budgets of ρ_v and ρ_H in domain Δ is generally larger than the contribution of $\rho_{v\_tagged\_\delta}$ and $\rho_{H\_tagged\_\delta}$ to the budgets of ρ_v and ρ_H in domain δ, although with a similar time-height sign distribution (compare Figures 5e–5h and Figures 11e–11h, Figures 6f–6j and Figures 12f–12j). Additionally, the weak and intermittent positive layer in the horizontal transport term of the budget of $\rho_{v\_tagged\_\Delta}$ at 2–4 km is better defined (compare Figure 5f and Figure 11f). This particular feature suggests that the atmospheric water pathway from *Knoche and Kunstmann* [2013], i.e., tagged water transported back to domain Δ by the mid-level West African easterlies after low level northeasterly transport by the oceanic monsoon flow and convective lifting outside of domain Δ, does play a larger role in domain Δ, as compared to that in domain δ.

A β_{tagged_Δ} of about 11.8% is obtained for the simulated period March–October 2003 (see Figure 14 and Table 2), which is significantly higher than the 7.3% obtained for β_{bulk_Δ} (Table 2). There is indeed a significant inflow of tagged water (see yellow solid line with diamonds in Figure 13b), a potential source of discrepancy in the bulk method [*Schär et al.*, 1999]. At the monthly scale, β_{tagged_Δ} and β_{bulk_Δ} are close in March, 4.7 and 4.5%, respectively, although β_{tagged_Δ} is comparatively much higher in the following months (see Figure 14b). At the daily scale, β_{tagged_Δ} displays oscillations between 3 and 21% that β_{bulk_Δ} does not pick up (Figure 14a).

5.2.3. Effect of Nonwell Vertical Mixing and Return Flow

As for domain δ (section 4.2.3), differences between β_{tagged_Δ} and β_{bulk_Δ} in domain Δ are investigated with equation (11) (Figure 14 and Table 2). ε_{I_Δ}, ε_{O_Δ} and ε_{W_Δ} all contribute significantly to the larger daily

variations in β_{tagged_Δ} (Figure 14a). Also, the contribution of ε_{W_Δ} at the daily scale almost completely vanishes at the monthly scale (see light blue circles in Figure 14b). In comparison to ε_{I_δ} and ε_{O_δ}, ε_{I_Δ} and ε_{O_Δ} are relatively large in March (compare yellow diamonds and red squares in Figures 10 and 14). Domain Δ is indeed closer to the Guinean coast, so that oceanic southwesterlies are more prone to increase vertical wind shear condition in domain Δ in March as well. The positive contribution from ε_{I_Δ} is however counterbalanced by a negative contribution from ε_{O_Δ}, leading to a β_{bulk_Δ} relatively close to β_{tagged_Δ} for this month. This means that the bulk and tagging methods give a similar precipitation ratio in this case, because the nonverified assumptions in the bulk method, i.e., no return flow and well vertical mixing, give cancelling errors.

For the period March–October 2003, as shown in Table 3, the 11.8% of β_{tagged_Δ} is distributed in 61.9% of β_{bulk_Δ}, 24.8% of ε_{I_Δ}, 13.6% of ε_{O_Δ}, 0% of ε_{W_Δ} and -0.1% of the residual term. Assuming this residual term can be distributed to each of the right hand side terms in equation (11), the contribution of return flow and nonwell vertically mixed outflow to regional precipitation recycling in domain Δ is about 25 and 14%, respectively. The fact that ε_{I_Δ} has a larger contribution as compared to that of ε_{I_δ} (see Table 2), and the relatively small contribution of the residual term, further supports the conclusion that the atmospheric water pathway from *Knoche and Kunstmann* [2013] does play a larger role in precipitation recycling in domain Δ, as compared to that in domain δ. This suggests that the well-known scale-dependency of regional precipitation recycling [e.g., *Trenberth*, 1999; *Van der Ent and Savenije*, 2011], i.e., the larger the area the larger the precipitation recycling ratio, is strengthened in West Africa due to this atmospheric pathway.

6. Summary and Conclusion

Two methods to quantify the atmospheric branch of the water cycle and regional precipitation recycling have been implemented in the WRF model and tested for the West African region. First, the *E*-tagging method of *Knoche and Kunstmann* [2013] has been adapted to the WRF modeling system, which provides the so-called tagging precipitation recycling ratio β_{tagged}. Second, the budgets of total and tagged atmospheric water vapor and hydrometeors have been added to the model, using a similar method as that of *Arnault* [2013] for the budget of momentum, which allow quantifying atmospheric processes playing a role in the production of simulated precipitation. These three-dimensional budgets are used to derive the budget of bulk atmospheric moisture from *Schär et al*. [1999] and write β_{tagged} as a function of the so-called bulk precipitation recycling ratio β_{bulk}, and three additional terms quantifying the effect of return flow and nonwell vertical mixing (equation (11)).

A WRF simulation has been conducted for the wet season 2003 in West Africa, using a single domain at 10 km resolution and ERA-Interim reanalyzes for the initial and lateral boundary condition. Regional precipitation recycling was investigated in a 100×100 km^2 area around (11.5°N 1.5°S), i.e., domain δ, and in a 1000×1000 km^2 area centered on domain δ, i.e., domain Δ. According to the budgets of water vapor and hydrometeors, it was found that a prerequisite condition for evaporated water to participate to the precipitation process in domain δ and Δ was that it is lifted to the mid-levels.

The budgets of tagged water vapor and hydrometeors originating from domain δ showed that locally evaporated water was mainly transported outside of domain δ in the low levels. Still, a small proportion was transported upward within domain δ through convective lifting, leading to a β_{tagged_δ} of 1.2% for the whole simulated period. The bulk method slightly underestimated this value, i.e., β_{bulk_δ} was about 0.9%, due to the neglected contribution of outflow nonwell vertical mixing and return flow. This is in association with low-level southwesterlies and mid-level easterlies prevailing in West Africa during the wet season. The budgets of tagged water vapor and hydrometeors originating from domain Δ displayed similar features, except with higher amplitudes. Accordingly, β_{tagged_Δ} was about 11.8% for the whole simulated period, although β_{bulk_Δ} was only 7.3%. This smaller value was associated with a relatively higher contribution of return flow in the case of domain Δ, suggesting that the atmospheric pathway from *Knoche and Kunstmann* [2013] strengthens the well-known scale-dependency of the regional precipitation recycling [e.g., *Trenberth*, 1999; *Van der Ent and Savenije*, 2011], i.e., the larger the area the larger the precipitation recycling ratio.

This model study confirms previous findings that local *E* in West Africa is not the dominant factor controlling local precipitation, even at the 1000×1000 km^2 scale [e.g., *Druyan and Koster*, 1989; *Knoche and Kunstmann*, 2013]. Still, as in *Kunstmann and Jung* [2007], regional precipitation recycling was found to increase

with *E* (i.e., increase of soil moisture), suggesting some potential impact of land management on West African precipitation. As shown by *Goessling and Reick* [2011] in a global numerical experiment, changes in *E* at a sufficiently large scale also have the potential to affect the atmospheric circulation, and precipitation in this case is much more sensitive to *E*-induced changes in the atmospheric circulation than to changes in *E* itself. The role of land surface changes on the atmospheric circulation should therefore be further investigated in order to better assess the potential impact of land management on West African precipitation [e.g., *Hagos et al*., 2014; *Im et al*., 2014].

The newly developed *E*-tagging and budget methods within WRF are general enough to quantify the impact of land surface changes on such precipitation-related atmospheric dynamic mechanisms. These methods can be used to quantify and further understand the atmospheric part of land-atmosphere feedback mechanisms for different spatial and temporal scales and for different climate regions worldwide.

Acknowledgements
This study is part of the core research program of the West African Service Center on Climate Change and Adaptive Land Use (WASCAL) funded by the German Ministry of Education and Research. TRMM precipitation data were obtained online at http://mirador.gsfc.nasa.gov/cgi-bin/mirador/homepageAlt.pl?keyword=TRMM_3B42. Test simulations were run at the German Climate Computing Center. Thanks go to Junhong Lee and Ui-Yong Byun from the Yonsei University, South Korea, for sharing ideas on the topic of atmospheric water tracking during their visit in Garmisch-Partenkirchen in February 2015, and to the associate editor and three reviewers for their constructive remarks.

References

Arnault, J. (2013), Large-scale dynamical influence of a gravity wave generated over the Antarctic Peninsula––Regional modelling and budget analysis, *Tellus, Ser. A*, *65*, 1–24, doi:10.3402/tellusa.v65i0.20254.

Bisselink, B., and A. Dolman (2008), Precipitation recycling: Moisture sources over Europe using ERA-40 data, *J. Hydrometeorol.*, *9*(5), 1073–1083, doi:10.1175/2008JHM962.1.

Bosilovich, M. G., and J. Chern (2006), Simulation of water sources and precipitation recycling for the MacKenzie, Mississippi, and Amazon River basins, *J. Hydrometeorol.*, *7*, 312–329, doi:10.1175/JHM501.1.

Bosilovich, M. G., and S. D. Schubert (2001), Precipitation recycling in the GEOS- 1 data assimilation system over the central United States, *J. Hydrometeorol.*, *2*, 26–35, doi:10.1175/1525-7541(2001)002 < 0026:PROTCU>2.0.CO;2.

Bosilovich, M. G., Y.C. Sud, S. D. Schubert, and G. K. Walker (2003), Numerical simulation of the large-scale North American monsoon water sources, *J. Geophys. Res.*, *108*(D16), 8614, doi:10.1029/2002JD003095.

Browne, N. A. K., and M. B. Sylla (2012), Regional climate model sensitivity to domain size for the simulation of the West African summer monsoon rainfall, *Int. J. Geophys.*, *2012*, 625831, doi:10.1155/2012/625831.

Brubaker, K. L., D. Entekhabi, and P. S. Eagleson (1993), Estimation of continental precipitation recycling, *J. Clim.*, *6*, 1077–1089, doi:10.1175/1520-0442(1993)006 < 1077:EOCPR>2.0.CO;2.

Burde, G. I., and A. Zangvil (2001), The estimation of regional precipitation recycling. Part I: Review of recycling models, *J. Clim.*, *14*, 2497–2508, doi:10.1175/1520-0442(2001)014 < 2497:TEORPR>2.0.CO;2.

Chen, F., and J. Dudhia (2001), Coupling an Advanced Land Surface-Hydrology Model with the Penn State-NCAR MM5 Modeling System. Part I: Model implementation and sensitivity, *Mon. Weather Rev.*, *129*, 569–585, doi:10.1175/1520-0493(2001)129 < 0569:CAALSH>2.0.CO;2.

Chen, F., and Y. Zhang (2009), On the coupling strength between the land surface and the atmosphere: From viewpoint of surface exchange coefficients, *Geophys. Res. Lett.*, *36*, L10404, doi:10.1029/2009GL037980.

Csiszar, I., and G. Gutman (1999), Mapping global land surface albedo from NOAA/AVHRR, *J. Geophys. Res.*, *104*, 6215–6228, doi:10.1029/1998JD200090.

Dee, D. P., et al. (2011), The ERA-Interim reanalysis: configuration and performance of the data assimilation system, *Q. J. R. Meteorol. Soc.*, *137*, 553–597, doi:10.1002/qj.828.

Dirmeyer, P. A., and K. L. Brubaker (1999), Contrasting evaporative moisture sources during the drought of 1988 and the flood of 1993, *J. Geophys. Res.*, *104*, 19,383–19,397, doi:10.1029/1999JD900222.

Dominguez, F., and P. Kumar (2008), Precipitation recycling variability and ecoclimatological stability: A study using NARR data. Part I: Central USA plains, *J. Clim.*, *21*, 5165–5186, doi:10.1175/2008JCLI1756.1.

Dominguez, F., P. Kumar, and E. R. Vivoni (2008), Precipitation recycling variability and ecoclimatological stability: A study using NARR data. Part II: North American monsoon region, *J. Clim.*, *21*, 5187–5203, doi:10.1175/2008JCLI1760.1.

Druyan, L. M., and R. D. Koster (1989), Sources of Sahel precipitation for simulated drought and rainy seasons, *J. Clim.*, *2*, 1438–1446, doi:10.1175/1520-0442(1989)002 < 1438:SOSPFS>2.0.CO;2.

Dudhia, J. (1989), Numerical study of convection observed during the Winter Monsoon Experiment using a mesoscale two-dimensional model, *J. Atmos. Sci.*, *46*, 3077–3107, doi:10.1175/1520-0469(1989)046 < 3077:NSOCOD>2.0.CO;2.

Eltahir, E. A. B., and R. L. Bras (1996), Precipitation recycling, *Rev. Geophys.*, *34*, 367–378, doi:10.1029/96RG01927.

Friedl, M. A., et al. (2002), Global land cover mapping from MODIS: algorithms and early results, *Remote Sens. Environ.*, *83*, 287–302, doi:10.1080/01431160608948707.

Gantner, L., and N. Kalthoff (2010), Sensitivity of a modelled life cycle of a mesoscale convective system to soil conditions over West Africa, *Q. J. R. Meteorol. Soc.*, *136*, 471–482, doi:10.1002/qj.425.

Gimeno, L., A. Stohl, R. M. Trigo, F. Domínguez, K. Yoshimura, L. Yu, A. Drumond, A. M. Durán-Quesada, and R. Nieto (2012), Oceanic and terrestrial sources of continental precipitation, *Rev. Geophys.*, *50*, RG4003, doi:10.1029/2012RG000389.

Goessling, H. F., and C. H. Reick (2011), What do moisture recycling estimates tell us? Exploring the extreme case of nonevaporating continents, *Hydrol. Earth Syst. Sci.*, *15*, 3217–3235, doi:10.5194/hess-15-3217-2011.

Goessling, H. F., and C. H. Reick (2013), On the "well-mixed" assumption and numerical 2-D tracing of atmospheric moisture, *Atmos. Chem. Phys.*, *13*, 5567–5585, doi:10.5194/acp-13-5567-2013.

Grell, G., J. Dudhia, and D. Stauffer (1994), A description of the fifth- generation Penn State/NCAR mesoscale model (MM5), *NCAR Tech. Note NCAR/TN-398+STR*, NCAR, Boulder, Colo., doi:10.5065/D60Z716B.

Gutman, G., and A. Ignatov (1998), The derivation of the green vegetation fraction from NOAA/AVHRR data for use in numerical weather prediction models, *Int. J. Remote Sens.*, *19*(8), 1533–1543, doi:10.1080/014311698215333.

Hagos, S. M, L. Y. R. Leung, Y. Xue, A. Boone, F. de Sales, N. Neupane, M. Huang, and J. H. Yoon (2014), Assessment of uncertainties in the response of the African monsoon precipitation to land use change simulated by a regional model, *Clim. Dyn.*, *43*(9-10), 2765–2775, doi:10.1007/s00382-014-2092-x.

Hong, S.-Y., J. Dudhia, and S.-H. Chen (2004), A revised approach to ice microphysical processes for the bulk parameterization of clouds and precipitation, *Mon. Weather Rev.*, *132*, 103–120, doi:10.1175/1520-0493(2004)132 < 0103:ARATIM>2.0.CO;2.
Hong, S.-Y., Y. Noh, and J. Dudhia (2006), A new vertical diffusion package with an explicit treatment of entrainment processes, *Mon. Weather Rev.*, *134*, 2318–2341, doi:10.1175/MWR3199.1.
Huffman, G. J., R. F. Adler, D. T. Bolvin, G. Gu, E. J. Nelkin, K. P. Bowman, Y. Hong, E. F. Stocker, and D. B. Wolff (2007), The TRMM Multi-satellite precipitation analysis: Quasi-global, multi-year, combined-sensor precipitation estimates at fine scale, *J. Hydrometeorol.*, *8*, 38–55, doi:10.1175/JHM560.1.
Im, E. S., M. P. Marcella, and E. A. B. Eltahir (2014), Impact of potential large-scale irrigation on the West African monsoon and its dependence on location of irrigated area, *J. Clim.*, *27*, 994–1009, doi:10.1175/JCLI-D-13-00290.1.
Joussaume, S., R. Sadourny, and C. Vignal (1986), Origin of precipitating water in a numerical simulation of the July climate, *Ocean-Air Inter.*, *1*, 43–56.
Jung, M., M. Reichstein, and A. Bondeau (2009), Towards global empirical upscaling of FLUXNET eddy covariance observations: Validation of a model tree ensemble approach using a biosphere model, *Biogeosciences*, *6*, 2001–2013, doi:10.5194/bg-6-2001-2009.
Jung, M., et al. (2010), Recent decline in the global land evapotranspiration trend due to limited moisture supply, *Nature*, *467*(7318), 951–954, doi:10.1038/nature09396.
Klein, C., D. Heinzeller, J. Bliefernicht, and H. Kunstmann (2015), Variability of West African monsoon patterns generated by a WRF multi-physics Ensemble, *Clim. Dyn.*, *45*, 2733–2755, doi:10.1007/s00382-015-2505-5.
Knoche, H. R., and H. Kunstmann (2013), Tracking atmospheric water pathways by direct evaporation tagging: A case study for West Africa, *J. Geophys. Res. Atmos.*, *118*, 12,345–12,358, doi:10.1002/2013JD019976.
Koster, R., J. Jouzel, R. Suozzo, and G. Russell (1986), Global sources of local precipitation as determined by the NASA/GISS GCM, *Geophys. Res. Lett.*, *13*, 121–124, doi:10.1029/GL013i002p00121.
Kumar, A., F. Chen, M. Barlage, M. B. Ek, and D. Niyogi (2014), Assessing impacts of integrating MODIS vegetation data in the weather research and forecasting (WRF) model coupled to two different canopy-resistance approaches, *J. Appl. Meteorol. Climatol.*, *53*, 1362–1380, doi:10.1175/JAMC-D-13-0247.1.
Kunstmann, H., and G. Jung (2007), Influence of soil-moisture and land use change on precipitation in the Volta Basin of West Africa, *Int. J. River Basin Manage.*, *5*, 9–16, doi:10.1080/15715124.2007.9635.
Marsham, J. H., N. Dixon, L. Garcia-Carreras, G. M. S. Lister, D. J. Parker, P. Knippertz, and C. Birch (2013), The role of moist convection in the West African monsoon system: Insights from continental-scale convection-permitting simulations, *Geophys. Res. Lett.*, *40*, 1843–1849, doi:10.1002/grl.50347.
Mlawer, E. J., S. J. Taubman, P. D. Brown, M. J. Iacono, and S. A. Clough (1997), Radiative transfer for inhomogeneous atmosphere: RRTM, a validated correlated-k model for the long-wave, *J. Geophys. Res.*, *102*, 16,663–16,682, doi:10.1029/97JD00237.
Nicholson, S. (2000), Land surface processes and Sahel climate, *Rev. Geophys.*, *38*, 117–139, doi:10.1029/1999RG900014.
Nicholson, S. E., et al. (2003), Validation of TRMM and other rainfall estimates with a high-density gauge dataset for West Africa—Part II: Validation of TRMM rainfall products, *J. Appl. Meteorol.*, *42*, 1355–1368, doi:10.1175/1520-0450(2003)042 < 1355:VOTAOR>2.0.CO;2.
Pathak, A., S. Ghosh, and P. Kumar (2014), Precipitation recycling in the Indian subcontinent during summer monsoon, *J. Hydrometeorol.*, *15*, 2050–2066, doi:10.1175/JHM-D-13-0172.1.
Reisner, J., R. M. Rasmussen, and R. T. Bruintjes (1998), Explicit forecasting of supercooled liquid water in winter storms using the MM5 mesoscale model, *Q. J. R. Meteorol. Soc.*, *124*, 1071–1107, doi:10.1002/qj.49712454804.
Rios-Entenza, A., P. M. M. Soares, R. M. Trigo, R. M. Cardoso, and G. Miguez-Macho (2014), Moisture recycling in the Iberian Peninsula from a regional climate simulation: Spatiotemporal analysis and impact on the precipitation regime, *J. Geophys. Res. Atmos.*, *119*, 5895–5912, doi:10.1002/2013JD021274.
Savenije, H. H. G. (1995), Does moisture feedback affect rainfall significantly?, *Phys. Chem. Earth*, *20*(5–6), 507–513, doi:10.1016/S0079-1946(96)00014-6.
Schär, C., D. Lüthi, and U. Beyerle (1999), The soil-precipitation feedback: A process study with a regional climate model, *J. Clim.*, *12*, 722–741, doi:10.1175/1520-0442(1999)012 < 0722:TSPFAP>2.0.CO;2.
Skamarock, W. C., and J. B. Klemp (2008), A time-split nonhydrostatic atmospheric model for weather research and forecasting applications, *J. Comput. Phys.*, *227*, 3465–3485, doi:10.1016/j.jcp.2007.01.037.
Sodemann, H., H. Wernli, and C. Schwierz (2009), Sources of water vapour contributing to the Elbe flood in August 2002—A tagging study in a mesoscale model, *Q. J. R. Meteorol. Soc.*, *135*, 205–223, doi:10.1002/qj.374.
Taylor, C. M., D. J. Parker, and P. P. Harris (2007), An observational case study of mesoscale atmospheric circulations induced by soil moisture, *Geophys. Res. Lett.*, *34*, L15801, doi:10.1029/2007GL030572.
Taylor, C. M., A. Gounou, F. Guichard, P. P. Harris, R. J. Ellis, F. Couvreux, and M. De Kauwe (2011a), Frequency of Sahelian storm initiation enhanced over mesoscale soil-moisture patterns, *Nat. Geosci.*, *4*, 430–433, doi:10.1038/ngeo1173.
Taylor, C. M., et al. (2011b), New perspectives on land–atmosphere feedbacks from the African Monsoon Multidisciplinary Analysis, *Atmos. Sci. Lett.*, *44*, 38–44, doi:10.1002/asl.336.
Thiemig, V., R. Rojas, M. Zambrano-Bigiarini, V. Levizzani, and A. De Roo (2012), Validation of satellite-based precipitation products over sparsely gauged African river basins, *J. Hydrometeorol.*, *13*, 1760–1783, doi:10.1175/JHM-D-12-032.1.
Trenberth, K. E. (1999), Atmospheric moisture recycling: Role of advection and local evaporation, *J. Clim.*, *12*, 1368–1381, doi:10.1175/1520-0442(1999)012 < 1368:AMRROA>2.0.CO;2.
Van der Ent, R. J., and H. H. G. Savenije (2011), Length and time scales of atmospheric moisture recycling, *Atmos. Chem. Phys.*, *11*, 1853–1863, doi:10.5194/acp-11-1853-2011.
Van der Ent, R. J., H. H. G. Savenije, B. Schaefli, and S. C. Steele-Dunne (2010), Origin and fate of atmospheric moisture over continents, *Water Resour. Res.*, *46*, W09525, doi:10.1029/2010WR009127.
Van der Ent, R. J., O. A. Tuinenburg, H. R. Knoche, H. Kunstmann, and H. H. G. Savenije (2013), Should we use a simple or complex model for moisture recycling and atmospheric moisture tracking?, *Hydrol. Earth Syst. Sci.*, *17*, 4869–4884, doi:10.5194/hess-17-4869-2013.
Wei, J., H. Knoche, and H. Kunstmann (2015), Contribution of transpiration and evaporation to precipitation: An ET-Tagging study for the Poyang Lake region in Southeast China, *J. Geophys. Res. Atmos.*, *120*, 6845–6864, doi:10.1002/2014JD022975.